JACC: BASIC TO TRANSLATIONAL SCIENCE VOL. 7, NO. 5, 2022

PRECLINICAL RESEARCH

Cardiac Mesenchymal Stem Cells Promote Fibrosis and Remodeling in Heart Failure

Role of PDGF Signaling

Tariq Hamid, PhD,[a,b] Yuanyuan Xu, PhD,[b] Mohamed Ameen Ismahil, PhD,[a,b] Gregg Rokosh, PhD,[a,b] Miki Jinno, BS,[b] Guihua Zhou, MD, PhD,[b] Qiongxin Wang, PhD,[a,b] Sumanth D. Prabhu, MD[a,b,c]

VISUAL ABSTRACT

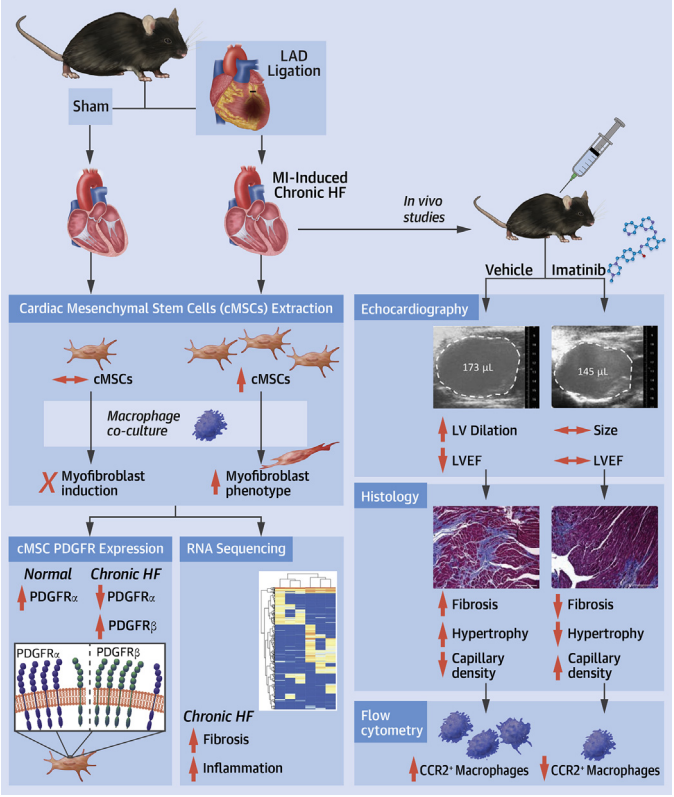

Hamid T, et al. J Am Coll Cardiol Basic Trans Science. 2022;7(5):465-483.

HIGHLIGHTS

- **Resident cMSCs comprise a distinct mesenchymal population that is temporally expanded and exhibit pro-fibrotic and pro-inflammatory features in failing hearts.**
- **cMSCs in failing hearts undergo a phenotypic switch characterized by enhanced pro-inflammatory and pro-fibrotic responses.**
- **Pro-inflammatory macrophages promote a myofibroblast differentiation fate of cMSCs from failing hearts, in part mediated by PDGF/PDGF receptor β activation.**
- **Pharmacologic PDGF receptor inhibition in a mouse model of myocardial infarction alleviated long-term cardiac remodeling, inflammation, hypertrophy, and fibrosis and increased myocardial capillary density.**
- **Inhibiting the pathologic cMSC phenotype, or restoring a normal cMSC phenotype, may combat the progression of cardiac fibrosis and failure after myocardial infarction.**

From the [a]Division of Cardiology, Washington University School of Medicine, St. Louis, Missouri, USA; [b]Division of Cardiovascular Disease, University of Alabama at Birmingham, Birmingham, Alabama, USA; and the [c]Birmingham VAMC, Birmingham, Alabama, USA.

The authors attest they are in compliance with human studies committees and animal welfare regulations of the authors' institutions and Food and Drug Administration guidelines, including patient consent where appropriate. For more information, visit the Author Center.

Manuscript received April 21, 2021; revised manuscript received January 11, 2022, accepted January 11, 2022.

ISSN 2452-302X https://doi.org/10.1016/j.jacbts.2022.01.004

JACC: BASIC TO TRANSLATIONAL SCIENCE VOL. 7, NO. 5, 2022
MAY 2022:465–483

ABBREVIATIONS AND ACRONYMS

α-SMA = alpha smooth muscle actin

CCL = C-C motif chemokine ligand

CCR2 = C-C chemokine receptor 2

cDNA = complementary DNA

cMSC = cardiac mesenchymal stem cell

DDR2 = discoidin domain receptor 2

DMEM = Dulbecco's modified Eagle medium

EDV = end-diastolic volume

EF = ejection fraction

ESV = end-systolic volume

HF = heart failure

IL = interleukin

INF = interferon

LV = left ventricular

MI = myocardial infarction

mRNA = messenger RNA

MSC = mesenchymal stem cell

PBS = phosphate-buffered saline

PCR = polymerase chain reaction

PDGF = platelet-derived growth factor

PDGFR = platelet-derived growth factor receptor

Lin = lineage

siRNA = small interfering RNA

TGFβ = transforming growth factor beta

WGA = wheat germ agglutinin

SUMMARY

Heart failure (HF) is characterized by progressive fibrosis. Both fibroblasts and mesenchymal stem cells (MSCs) can differentiate into pro-fibrotic myofibroblasts. MSCs secrete and express platelet-derived growth factor (PDGF) and its receptors. We hypothesized that PDGF signaling in cardiac MSCs (cMSCs) promotes their myofibroblast differentiation and aggravates post-myocardial infarction left ventricular remodeling and fibrosis. We show that cMSCs from failing hearts post-myocardial infarction exhibit an altered phenotype. Inhibition of PDGF signaling in vitro inhibited cMSC–myofibroblast differentiation, whereas in vivo inhibition during established ischemic HF alleviated left ventricular remodeling and function, and decreased myocardial fibrosis, hypertrophy, and inflammation. Modulating cMSC PDGF receptor expression may thus represent a novel approach to limit pathologic cardiac fibrosis in HF. (J Am Coll Cardiol Basic Trans Science 2022;7:465-483) © 2022 The Authors. Published by Elsevier on behalf of the American College of Cardiology Foundation. This is an open access article under the CC BY-NC-ND license (http://creativecommons.org/licenses/by-nc-nd/4.0/).

Heart failure (HF) is a state of chronic inflammation.[1,2] Analogous to many chronic inflammatory diseases, failing hearts also exhibit increased fibrosis[2] and myofibroblast activation.[3,4] Overt fibrotic responses in HF contribute to impaired cardiac function and failure.[5,6] Although fibroblasts are classically considered the main cellular precursor of myofibroblasts,[7,8] mesenchymal stem cells (MSCs) residing in several organs, including the adult heart,[9,10] can also differentiate into myofibroblasts to affect fibrosis, such as after acute myocardial infarction (MI).[11,12] Importantly, however, the pathophysiological role of resident cardiac MSCs (cMSCs) in the genesis of fibrotic responses in the chronically failing heart is unknown.

Failing hearts are characterized by increased pro-inflammatory macrophage infiltration that promotes adverse cardiac remodeling and function,[1,2,13] in part by activation of the extracellular matrix modifying myofibroblasts that promote pathologic fibrosis.[3] Little is known, however, about how inflammatory macrophages affect the differentiation and functional outcomes of resident MSCs in failing hearts, and whether modulation of cMSCs via their interactions with macrophages can modify subsequent cMSC-derived fibrotic responses. In this regard, platelet-derived growth factor (PDGF) is an important protein mediator of tissue fibrosis, and both MSCs and macrophages secrete PDGF and express PDGF receptors (PDGFRs).[14,15] Overexpression of PDGFR ligands induces cardiac dysfunction and fibrosis,[16-18] whereas inhibition of PDGFR signaling attenuates left ventricular (LV) remodeling and fibrosis in animal models of reperfused MI, β-adrenergic activation, and myocarditis.[19-21] However, whether and how cMSC-localized PDGFR signaling influences cMSC function and differentiation in the failing heart are unknown. Accordingly, we defined alterations in the cMSC profile in HF to better understand the effect of the pathologic cardiac microenvironment on cMSC biology and function, the potential contributory effects of macrophage-cMSC interaction and PDGFR signaling to these changes, and the pathophysiological role of cMSCs in the attendant cardiac dysfunction, remodeling, and fibrosis in chronic ischemic HF.

METHODS

MOUSE MI MODEL AND EXPERIMENTAL PROTOCOL.

All studies were performed in compliance with the National Research Council's Guide for the Care and Use of Laboratory Animals (revised 2011). Male C57BL/6J mice (The Jackson Laboratory; stock #000664) 10 to 12 weeks of age were used. After general anesthesia and left thoracotomy, MI was induced by permanent left coronary artery ligation as previously described.[2,22-24] Sham-operated mice were used as controls. Mice were assessed at 2 weeks' post-MI by echocardiography, and mice with comparable degrees of scar size (40%-50% of short-axis circumference) and LV remodeling were randomized to receive either the PDGFR inhibitor imatinib mesylate (30 mg/kg; Santa Cruz Biotechnology) or phosphate-buffered saline (PBS) vehicle (200 μL/injection) intraperitoneally every day for 3 weeks. The imatinib dose was based on previous studies in rodent models of myocarditis and hypertension[19,25] and murine dose equivalency calculations of clinically approved doses in humans.[26] After 3 weeks of treatment, echocardiography was repeated, and the mice were sacrificed.

Heart tissue was processed for mononuclear cell isolation and quantitative analysis of cMSCs and immune cells by flow cytometry, or fixed for histologic analyses as previously described.[2,24,27] These studies were approved by the University of Alabama at Birmingham Institutional Animal Care and Use Committee.

ECHOCARDIOGRAPHY. After anesthetic induction with tribromoethanol (0.25 mg/g intraperitoneally) and maintenance with 1% to 2% inhaled isoflurane, echocardiography was performed by using a VisualSonics Vevo 3100 High-Resolution System and MX400 scan head as previously described.[2,22,23,27] The mice were imaged on a heated bench-mounted adjustable rail system (Vevo Imaging Station) that allowed steerable and hands-free manipulation of the ultrasound transducer.

EXPANSION AND CHARACTERIZATION OF cMSCs. cMSCs were isolated from sham-operated and HF mice (8 weeks' post-MI) using primary explant cell outgrowth culture. Cell outgrowths from minced myocardial tissue were cultured in cMSC media (Dulbecco's modified Eagle medium [DMEM]/Ham's F-12 culture medium [Thermo Fisher Scientific-HyClone] supplemented with 0.2 mM L-glutathione, 10 ng/mL leukemia inhibitory factor, 10 ng/mL basic fibroblast growth factor, 10% fetal bovine serum, and 1% penicillin-streptomycin). Lineage-positive (Lin^+) cells ($CD5^+$, $CD45R^+$, $Cd11b^+$, $Gr\text{-}1^+$, $TER\text{-}119^+$; Miltenyi Biotec, #130-092-613), endothelial cells ($CD31^+$; BD, #553372), and fibroblasts (discoidin domain receptor 2 positive [$DDR2^+$]; LSBio, #LS-C255961) were depleted from explant cultures by using antibody-conjugated magnetic microbeads. After depletion, $Lin^-CD31^-DDR2^-$ cells were minimally expanded and further sorted by using a specific Sca1 antibody (eBioscience, #25-5981-81) and consequently enriched for $Sca1^+$ cells. $Lin^-CD31^-DDR2^-Sca1^+$ cells were minimally expanded and used at cell passages 3 to 5 for all experiments. cMSCs were evaluated for their ability to differentiate into adipogenic, osteogenic, and chondrogenic lineages using standard differentiation protocols.[9] Lineage-specific gene expression was used to confirm successful differentiation as described.[9,28]

IMMUNOPHENOTYPING OF cMSCs. cMSCs were evaluated for the expression of previously validated MSC surface markers[29] by flow cytometry using fluorophore-labeled primary antibodies against CD90 (BD, #553006), CD44 (eBioscience, #14-0441-81), CD49 (eBioscience, #13-0495-80), CD29 (eBioscience, #13-0291-82), CD73 (eBioscience, #12-0731-81), and CD105 (eBioscience, #12-1051-81).

MOUSE INFLAMMATION ANTIBODY ARRAY. The baseline inflammatory protein secretory profile of sham cMSCs and HF cMSCs was determined in conditioned media collected from cultured cMSCs. We used the Mouse Inflammation Array C1 (RayBiotech), which detects 40 murine inflammatory molecules in an antibody-based chemiluminescence detection system. Briefly, after blocking and washing of the antibody array, 1 mL of cMSC-conditioned media was added and incubated overnight at 4°C. After binding and washing, the array was incubated overnight at 4°C with the cocktail of provided biotinylated detection antibodies. Subsequent washing to remove the unbound antibodies was followed by incubation with horseradish peroxidase–conjugated streptavidin and chemiluminescence imaging. Arrays were imaged and analyzed by using Image J software (National Institutes of Health) and reported as arbitrary densitometric units.

COLLAGEN GEL CONTRACTION ASSAY. cMSCs were cultured to ~75% confluency. After trypsinization, washing, and cell counting, cMSCs (1×10^6 cells/mL) were resuspended in DMEM media containing 10% fetal bovine serum and mixed with a solution containing Type I rat tail collagen (Thermo Fisher Scientific), 5X PBS, and 50 mM sodium hydroxide on ice in a volume ratio of 3.3:3.3:2:1.3 mL, respectively. Next, 300 μL per well of this mixture (containing 1×10^5 cMSCs) was plated in a 48-well tissue culture plate and incubated at 37°C for 30 minutes to induce gelation. After gelation, 300 μL of DMEM + 10% fetal bovine serum was added, and the cells were cultured overnight. For co-culture experiments, RAW 264.7 (ATCC TIB-71) mouse macrophage cells were polarized in vitro either to an M1 phenotype upon treatment with lipopolysaccharide (1 μg/mL) and interferon-γ (4 ng/mL) or to an M2 phenotype upon treatment with interleukin (IL)-4 (10 ng/mL) or IL-10 (10 ng/mL) for 4 hours followed by washing in serum-free DMEM media and cell counting. Polarized macrophages (2×10^5 cells) were then added to the collagen mixture (described earlier). After overnight incubation, the cells were treated as indicated and cultured at 37°C in a 5% carbon dioxide incubator for 4 days with medium change at day 2. In some experiments, cMSC contraction assays were performed with the addition of conditioned media from polarized mouse RAW 264.7 macrophages. In studies of PDGFR inhibition, imatinib mesylate (10 μM; Santa Cruz Biotechnology) was added to the regimen after overnight culture of cells in collagen gels. On day 5, the collagen gels were detached from the culture wells by using a pipette tip, and the gel contraction was measured after overnight incubation. Collagen

JACC: BASIC TO TRANSLATIONAL SCIENCE VOL. 7, NO. 5, 2022
MAY 2022:465–483

gels were imaged by using a digital camera, and images were analyzed for total area by using Image J software. The results were expressed are percent change in area relative to the control undifferentiated group.

TRANSWELL MIGRATION ASSAY. Macrophage migration assays were performed by using Transwell inserts (6.5 mm, 8 μm pore size; Corning). Mouse RAW 264.7 (ATCC TIB-71) macrophages were polarized to an M1 phenotype (described earlier). M1-polarized macrophages (7.5×10^4 cells) were added to Transwell inserts containing 100 μL of serum-free DMEM media and placed into chambers containing sham cMSCs and HF cMSCs (1×10^5 cells) that were cultured overnight in cMSC media. Macrophages were allowed to migrate through the Transwell membrane for 2 to 6 hours in a cell culture incubator. In some experiments, macrophage-loaded inserts were instead exposed to conditioned media collected from cMSCs after 24 hours of culture. After co-culture, inserts were removed, washed with PBS, fixed with 3.7% paraformaldehyde for 10 minutes, and stained with wheat germ agglutinin (WGA) and 4′,6-diamidino-2-phenylindole for 30 minutes in the dark. After staining, nonmigrating cells on the upper surface of the inserts were removed with a cotton swab. Migrated cells on the bottom surface of the inserts were imaged and counted in 4 different microscopic fields. Data are expressed as mean ± SD of 2 independent experiments with 4 replicates per group.

RNA INTERFERENCE AND IMMUNOBLOTTING. cMSCs were transfected with 30 nM mouse PDGFRβ (or control) small interfering RNA (siRNA) (Santa Cruz Biotechnology) using INTERFERin siRNA transfection reagent (Polyplus Transfection) according to the manufacturer's instructions. After 96 hours of transfection, cMSCs were evaluated for PDGFRβ expression by immunoblotting using standard protocols as previously described.[22,23] In other experiments, siRNA-transfected cMSCs were trypsinized, washed, and counted 24 hours' post-transfection followed by the collagen gel contraction assay as described earlier. Primary antibodies used for immunoblotting were purchased from Santa Cruz Biotechnology, including against PDGFRα (sc-338), PDGFRβ (sc-432), alpha smooth muscle actin (α-SMA) (sc-58669), α-tubulin (sc-8035), vinculin (sc-736), and glyceraldehyde-3-phosphate dehydrogenase (sc-32249).

ISOLATION OF MONONUCLEAR CELLS AND FLOW CYTOMETRY. Mononuclear cells were isolated from the heart as previously described.[2,24,27,28] Isolated cell suspensions were incubated for 1 hour at room temperature in a cocktail of fluorophore-labeled antibodies to label cardiac macrophages, resident cMSCs, and cMSC-derived myofibroblasts. The following antibodies (from eBioscience, unless otherwise specified) were used: CD45-605 NC (30-F11), MerTK-APC (FAB5912A, R and D Systems), MHCII-eFluor450 (48-5320-82), Ly6C-PE/Cy7 (HK1.4), F4/80-eFluor 450 (BM8), F4/80-PerCP-Cyanine5.5 (45-4801-82), C-C chemokine receptor 2 (CCR2)-fluorescein isothiocyanate (FAB5538F, R and D Systems), LY-6A/E(Sca-1; 17-5981-81), CD31(BD, #553372), DDR2 (LSBio, #LS-C255961), and α-SMA (Santa Cruz; Sc-58669). CD45 was used to identify leukocytes, and macrophages were considered as $CD45^+MerTK^+MHCII^+Ly6C^-F4/80^+$ cells. Within this population, infiltrating (monocyte derived) and resident macrophages were defined as $CCR2^+$ or $CCR2^-$ cells, respectively. cMSCs were defined as $CD45^-Sca1^+CD31^-DDR2^-$ cells and cMSC-derived myofibroblasts as $CD45^-Sca1^+CD31^-DDR2^-\alpha\text{-}SMA^+$ cells.

Data were acquired on an LSRII flow cytometer (BD Biosciences) and analyzed with FlowJo software version 10.0.6 (FlowJo LLC). Cell populations were normalized to the total mononuclear cell population (frequency) or expressed as absolute numbers.

REAL TIME RT-PCR. Quantitative RT-PCR (reverse transcription polymerase chain reaction) to evaluate messenger RNA (mRNA) expression was performed as described previously.[2,22,23,28] Briefly, TRIzol (Life Technologies) extracted total RNA was quantified by using a NanoDrop 1000 spectrophotometer (Thermo Fisher Scientific). Total RNA (250 ng) was subjected to complementary DNA (cDNA) synthesis by using the High Efficiency cDNA Synthesis Kit (Invitrogen). The levels of various mRNA transcripts were determined by using Fast SYBR Green (Life Technologies) and gene-specific forward and reverse primer sets (**Table 1**) on a ViiA 7 RT-PCR instrument (Life Technologies). Then, 18S ribosomal RNA or β-actin expression was used to normalize mRNA expression levels by using the $\Delta\Delta C_T$ comparative method.

BULK cMSC RNA-SEQUENCING AND ANALYSIS. Live mononuclear cells isolated from chronic HF (or sham-operated) hearts (8 weeks' post-MI) were stained with SYTOX (live/dead staining) and CD45 and Sca1 antibodies. $SYTOX^-CD45^-Sca1^+$ cells were sorted on a BD FACS Aria flow cytometer. Using the SMART-Seq v4 Ultra Low Input RNA Kit (Takara Bio USA Inc), 250 cells were collected in lysis buffer at room temperature, pelleted, and processed for cDNA library preparation according to the kit protocol. Briefly, mRNA in cell lysates were reverse transcribed, and cDNA was prepared for amplification by template switching and extension. cDNA was amplified with 21 PCR cycles

and purified for Illumina Nextera DNA library construction and sequencing. STAR (version 2.5.3a) was used to align the raw RNA-sequencing FASTQ reads to the reference genome from Gencode.[30] Cufflinks was used on the STAR-aligned reads to assemble transcripts, estimate their abundances, and test for differential expression and regulation.[31,32] Cuffmerge was used to merge the assembled transcripts to a reference annotation and track Cufflinks transcripts across multiple experiments. Groups were compared by using an unpaired Student's *t*-test to assess statistical significance and adjusted *P* value corrected for multiple hypothesis testing with the Benjamini-Hochberg procedure. DESeq2 analyzed data were analyzed on the Ingenuity Pathway Analysis platform (Qiagen) to identify differentially regulated pathways. Heat maps were prepared by using $\log_2$-transformed normalized read counts using the *pheatmap* package within the R software (R Foundation for Statistical Computing, version R 4.0.0 GUI 1.71, 7827 Catalina build).

HISTOLOGY AND IMMUNOHISTOCHEMISTRY. Formalin-fixed, paraffin-embedded hearts from sham and HF mice were sectioned (5 μm), deparaffinized, and rehydrated. Immunohistological staining was performed as previously described.[2,22] Masson trichrome staining was used to quantify fibrosis while Alexa Fluor 488-conjugated WGA (Invitrogen) and 4′,6-diamidino-2-phenylindole staining were used to delineate cardiomyocytes and cell nuclei for measurement of cross-sectional area.

STATISTICAL ANALYSIS. Analyses were performed by using GraphPad Prism 8.0 (GraphPad Software). All data are expressed as mean ± SD. Two-group comparisons were made by using an unpaired Student's *t*-test for normally distributed variables. For comparisons of >2 groups, data were first assessed for normality by using the Shapiro-Wilk test. For normally distributed data, comparisons among multiple groups were evaluated by using 1- or 2-way analysis of variance, with Tukey's or Šidák's post hoc test analysis for multiple comparisons. For non-normal distribution, the data sets were logarithmically transformed, and if normality was satisfied, analysis of variance and Tukey's post-test were then performed. Changes in cardiac structure and function after imatinib treatment were evaluated by paired Student's *t*-test analysis. A *P* value <0.05 was considered statistically significant.

RESULTS

CHARACTERISTICS OF MOUSE RESIDENT cMSCs. cMSCs were isolated as cellular outgrowths from enzyme-perfused adult mouse hearts. Primary unsorted cMSCs were negative for c-kit expression but exhibited high expression (>70% of cells) of MSC markers Sca1, CD90, CD29, CD49, and CD44, while also expressing low levels (~2% of cells) of the fibroblast marker DDR2[33] and the endothelial cell marker CD31 (Figure 1A). After multiple rounds of depletion of hematopoietic cells (Lin^+, $CD45^+$), endothelial cells ($CD31^+$), and fibroblasts ($DDR2^+$), and enrichment for Sca1 expression, cMSCs ($Sca1^+Lin^-CD45^-CD31^-DDR2^-$) were minimally expanded and evaluated for in vitro capacity to differentiate into mesodermal lineages. Isolated cMSCs were able to differentiate into adipogenic, osteogenic, and chondrogenic lineages, as assessed by cell staining and gene expression markers (Supplemental Figure 1).

Next, we assessed cMSCs for the expression of fibroblast gene markers and performed myofibroblast phenotypic functional evaluation by using collagen gel contraction assays. As shown in Figure 1B, baseline expression of collagen-I, collagen-III, fibronectin, and α-SMA was substantially lower in cMSCs

TABLE 1 Forward and Reverse Primer Sequences Used for Reverse Transcription Polymerase Chain Reaction

Gene Name	Gene ID	Forward Sequence	Reverse Sequence
Collagen-I	12842	CTTCACCTACAGCACCCTT	TGACTGTCTTGCCCCAAAGT
Collagen-III	12825	TTCTGCCACCCCGAACTC	TTGCAGCCTTGGTTAGGATCA
Fibronectin	14268	AGGCAGAAAACAGGTCTCGATT	TGAATGAGTTGGCGGTGATATC
α-SMA (Acta2)	11475	CCTGACGCTGAAGTATCCGATAG	TTTTCCATGTCGTCCCAGTTG
Ccl6	20305	CCAGTGGTGGGTGCATCAA	GGGTTCCCCTCCTGCTGATA
Ccl7	6354	CCACATGCTGCTATGTCAAGA	ACACCGACTACTGGTGATCCT
Ccl12	20293	ATTTCCACACTTCTATGCCT	ATCCAGTATGGTCCTGAAG
TNFα	21929	CAGCCGATGGGTTGTACCTT	GGCAGCCTTGTCCCTTGA
iNOS (Nos2)	18126	AGACCTCAACAGAGCCCTCA	GCAGCCTCTTGTCTTTGACC
CD206 (Mrc1)	17533	CCCAAGGGCTCTTCTAAAGCA	CGCCGGCACCTATCACA
Arginase (Arg1)	11846	GCTCCAAGCCAAAGTCCTTAGA	CCTCGAGGCTGTCCTTTTGA
Cebpa (CEBPα)	12606	GCGAGCACGAGACGTCTATAGA	GCCAGGAACTCGTCGTTGAA
Alpl (ALP)	11647	ACCGCTGCCCGAATCC	TCTCCTCGCCCGTGTTGT
Runx2	12393	GCCGAGCTCCGAAATGC	AGATCGTTGAACCTGGCTACTTG
Fabp4 (Ap2)	11770	CCGCAGACGACAGGAAGGT	AGGGCCCCGCCATCT
Ccl2 (MCP-1)	20296	GTCTGTGCTGACCCCAAGAAG	TGGTTCCGATCCAGGTTTTTA
Acan (Agc1)	11595	ACGCCCCGGGAAGGT	CCGGATTCCGTAGGTTCTCA
Pdgfra	18595	GGCCGGGCCTCATCTC	TCATTCTCGTTTGGGAGGATAGA
Pdgfrb	18596	TGGGCAATGATGTGGTGAAC	ACCAGCCGCCCACTCTTC
Pdgfa	18590	GCTGCACTGGCTGTTGTAACA	GGTGGTGGACCCGTGAAG
Pdgfb	18591	CGCACAGAGGTGTTCCAGATC	CCAGGAAGTTGGCGTTGGT
Pdgfc	54635	ACCACGAGTCCTTCGGTGTT	GCATTGTTGAGCAGGTCCAA
Pdgfd	71785	TCCTCGCTTCCCGAACAG	ACGGAGCCACCATGTCAGA
Tlr2	24088	CCCTGTGCCACCATTTCC	GCCACGCCCACATCATTC
Tlr4	21898	ATGGCATGGCTTACACCAC	GAGGCCAATTTTGTCTCCAC
MMP10	17384	GCACCCTCAGGGACCAACT	CAGGAGTGGCCAAGTTCA
18s rRNA	19791	CGAACGTCTGCCCTATCAACTT	ACCCGTGGTCACCATGGTA
β-Actin (Actb)	11461	CGATGCCCTGAGGCTCTTT	TGGATGCCACAGGATTCCA
Vimentin	22352	GAGAGAGGAAGCCGAAAGCA	GCCAGAGAAGCATTGTCAACAT
Tenascin-C	21293	CCATCAGTACCACGGCTACCA	CGTCTGGAGTGGCATCTGAA

JACC: BASIC TO TRANSLATIONAL SCIENCE VOL. 7, NO. 5, 2022
MAY 2022:465–483

FIGURE 1 Characterization of Mouse Resident cMSCs

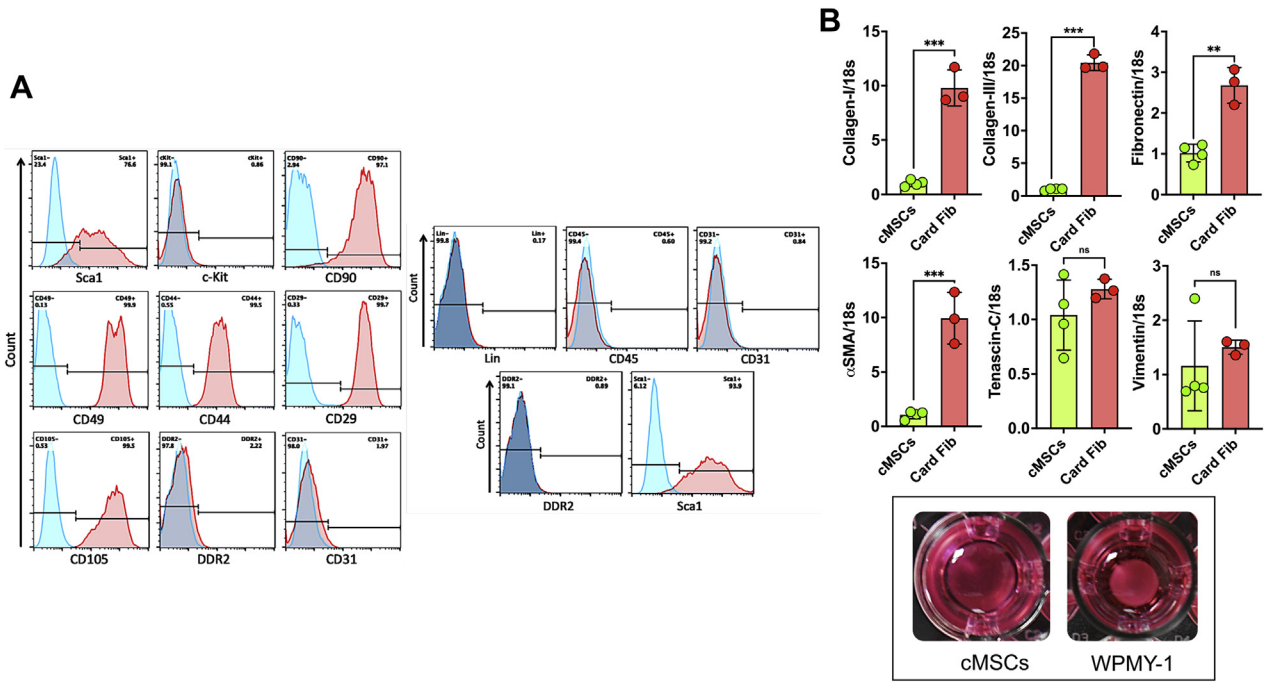

(A) Left panel: Representative histograms representing expression of mesenchymal stem cell (MSC) markers in minimally expanded primary cardiac MSC (cMSC) isolates (passages 2-4) analyzed by using flow cytometry. Shown also are the histograms **(blue shaded)** generated by using isotype controls for each marker analyzed. cMSCs expressed Sca1, CD90, CD49, CD44, CD29, and CD105; were negative for c-Kit expression; and exhibited low expression of discoidin domain receptor 2 (DDR2) and CD31. **Right panel:** Representative flow cytometry histograms depicting surface marker expression from cMSCs depleted for CD45, lineage markers (Lin), CD31, and DDR2 expression, and enriched for Sca1 expression using antibody-conjugated magnetic beads. **(B) Top:** Results of baseline gene expression of fibroblast markers collagen-I, collagen-III, fibronectin, alpha smooth muscle actin (α-SMA), and tenascin-C in sorted ($Lin^-CD45^-CD31^-DDR2^-Sca1^+$) cMSCs compared with expression in cardiac fibroblasts (Card Fib) isolated from wild-type adult mouse hearts. 18s ribosomal rRNA expression was used to normalize mRNA expression. Data were analyzed by using unpaired Student's *t*-test. n = 3 to 4 per group. **Bottom:** Representative images of the collagen gel contraction assay after overnight detachment of the collagen plugs after 4 days of myofibroblast differentiation using cMSCs **(left)** or commercially available WPMY-1 human prostrate stromal myofibroblast cell line **(right)**. $^{**}P < 0.01$, $^{***}P < 0.001$. ns = not significant.

compared with mouse cardiac fibroblasts. Mouse cardiac fibroblasts were isolated and cultured from adult wild-type mouse hearts as described by Kishore et al.[34] Moreover, cMSCs did not induce contraction of collagen gels; cMSC-imbued gels exhibited greater area than gels with the prostate myofibroblast cell line WPMY-1 (ATCC CRL-2854). Collectively, these data establish cMSCs as a distinct MSC population in the heart that do not harbor key features of fibroblasts or myofibroblasts at baseline.

cMSCs ARE EXPANDED IN CHRONIC HF. Using flow cytometry, we assessed cMSC abundance in C57BL/6 mouse hearts at early and late time points after a large nonreperfused MI. As previously shown, a progressive phenotype of HF with reduced ejection fraction (EF) is reliably produced in mice after nonreperfused MI,[2,22,27] which was confirmed by echocardiography. Figure 2 depicts representative flow cytometry gates of cardiac mononuclear cells and corresponding quantitation of $Sca1^-DDR2^+$ fibroblasts, total $Sca1^+$ cells, and $Sca1^+CD31^-DDR2^-$ cMSCs in mouse hearts after acute MI (1-day post-MI) and with chronic HF (8 weeks' post-MI). Acutely after MI (Figure 2A), there was a significant ~2-fold increase in cardiac fibroblasts compared with sham-operated hearts but comparable levels of total $Sca1^+$ cells and $Sca1^+$ cMSCs. In contrast, chronically failing hearts (Figure 2B) exhibited robust expansion of both total $Sca1^+$ cells (~8-fold increase) and $Sca1^+CD31^-DDR2^-$ cMSCs (~5.5-fold increase), but no difference in cardiac fibroblast number, compared with naive hearts.

Failing hearts are characterized by progressive fibrosis accompanied by myofibroblast proliferation. Although cardiac fibroblasts are considered their main cellular precursors,[35] MSCs can also differentiate into myofibroblasts.[11,12,36] Hence, we next

FIGURE 2 cMSCs and cMSC-Derived Myofibroblasts Are Increased in Chronic Heart failure

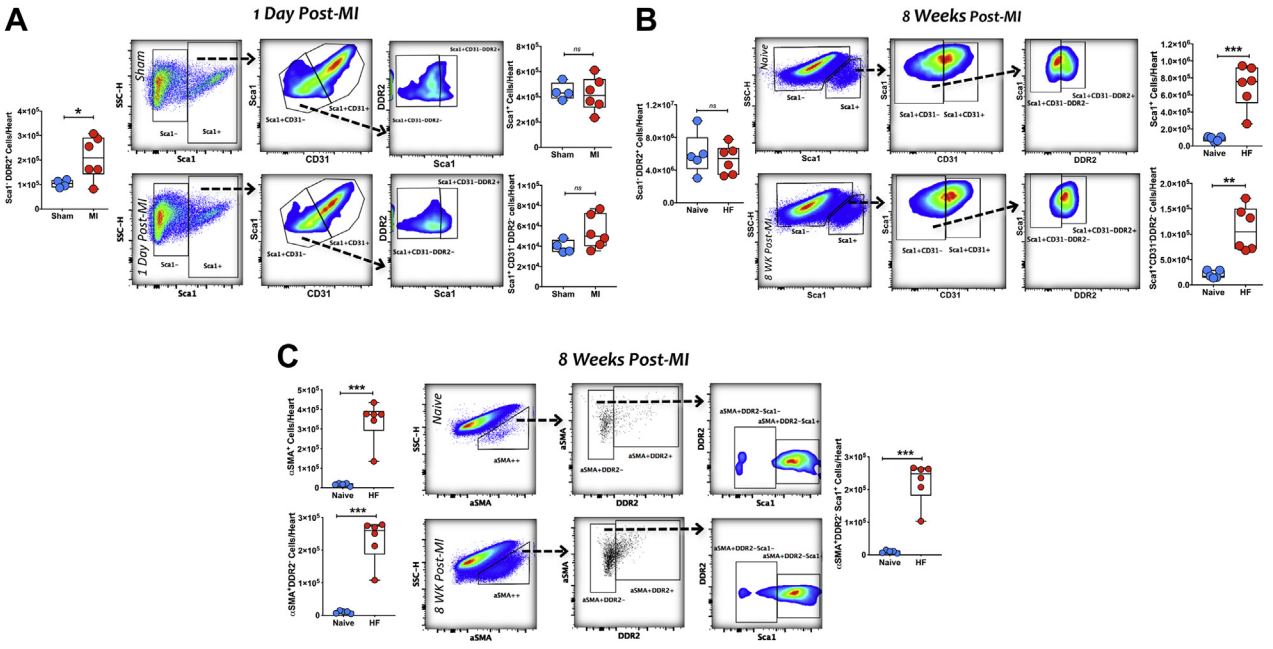

(A) Gating strategy for flow cytometric quantification of total Sca1$^+$ and Sca1$^-$CD31$^-$DDR2$^-$ cMSCs and Sca1-DDR2$^+$ cardiac fibroblasts in mouse hearts 1 day post-myocardial infarction (MI) (or sham operation). n= 4 to 6 per group. Data are expressed as cells per heart. *$P < 0.05$. **(B)** Flow cytometric gating and corresponding group data for assessment of cMSCs (Sca1$^+$CD31$^-$DDR2$^-$) and cardiac fibroblasts (Sca1$^-$DDR2$^+$) in mouse hearts 8 weeks' post-MI. Data are expressed as cells per heart. n = 5 to 6 per group. **$P < 0.005$, ***$P < 0.001$. **(C)** Flow cytometric gating strategy and group data for quantification of cMSC-derived myofibroblast in mouse hearts 8 weeks' post-MI. Myofibroblasts were identified based on a-SMA expression and classified as being derived from cMSCs based on their Sca1 expression. Data are expressed as cells per heart. n = 5 to 6 per group. ***$P < 0.001$. Statistical comparisons in all panels were performed by using the unpaired Student's t-test.
HF = heart failure; SSC-H = side scatter-height; other abbreviations as in Figure 1.

quantified the abundance of α-SMA-expressing, Sca1$^+$DDR2$^-$ myofibroblasts, which we considered as derived primarily from cMSCs, in the chronically failing heart. As illustrated in Figure 2C, compared with naive hearts, failing hearts exhibited markedly increased numbers of α-SMA$^+$DDR2$^-$Sca1$^+$ myofibroblasts (~20-fold increase), along with comparable robust increases in total α-SMA$^+$ and total α-SMA$^+$DDR2$^-$ cells. As shown Supplemental Figure 2, immunostaining revealed significant expansion of Sca1$^+$CD31$^-$DDR2$^-$ cMSCs in failing hearts, predominantly in border zone myocardium and also in the infarct scar, where they were found together with Sca1$^+$CD31$^+$DDR2$^-$ cells. Collectively, these results suggest that expanded cMSCs are an important source of myofibroblasts in the failing heart.

HF-DERIVED cMSCs EVIDENCE A PRO-INFLAMMATORY PHENOTYPE. Resident cMSCs were isolated from sham-operated and failing hearts (8 weeks' post-MI), expanded in culture, and used for experimentation between passages 3 and 5. cMSC secretory profiles were defined in conditioned media pooled from 3 cell isolates after 24 hours of culture using antibody-based arrays. HF cMSCs exhibited a pro-inflammatory secretome with increased levels of stromal cell-derived factor 1, C-C motif chemokine ligand (CCL) 11 (eotaxin-1), IL-6, and granulocyte-colony stimulating factor (Figure 3A). Furthermore, basal gene expression of chemokines CCL2, CCL6, CCL7, and CCL12 that recruit innate and adaptive immune cells was increased in HF cMSCs compared with sham cMSCs (Figure 3B).

We next determined the capacity of the cMSC secretome to polarize RAW 264.7 (RAW) macrophages in vitro. As shown in Figure 3C, RAW cells exposed to HF cMSC-conditioned media for 24 hours significantly upregulated genes associated with both M1 (inducible nitric oxide synthase, tumor necrosis factor, and Toll-like receptors 2 and 4) and M2 (CD206 and arginase) polarities vs exposure to either control or sham cMSC-conditioned media. cMSC-driven macrophage chemotaxis was evaluated by using a Transwell Migration assay. Compared with sham cMSCs, HF cMSCs significantly augmented M1-polarized RAW 264.7 macrophage migration

FIGURE 3 HF-Derived cMSCs Exhibit a Pro-inflammatory Phenotype

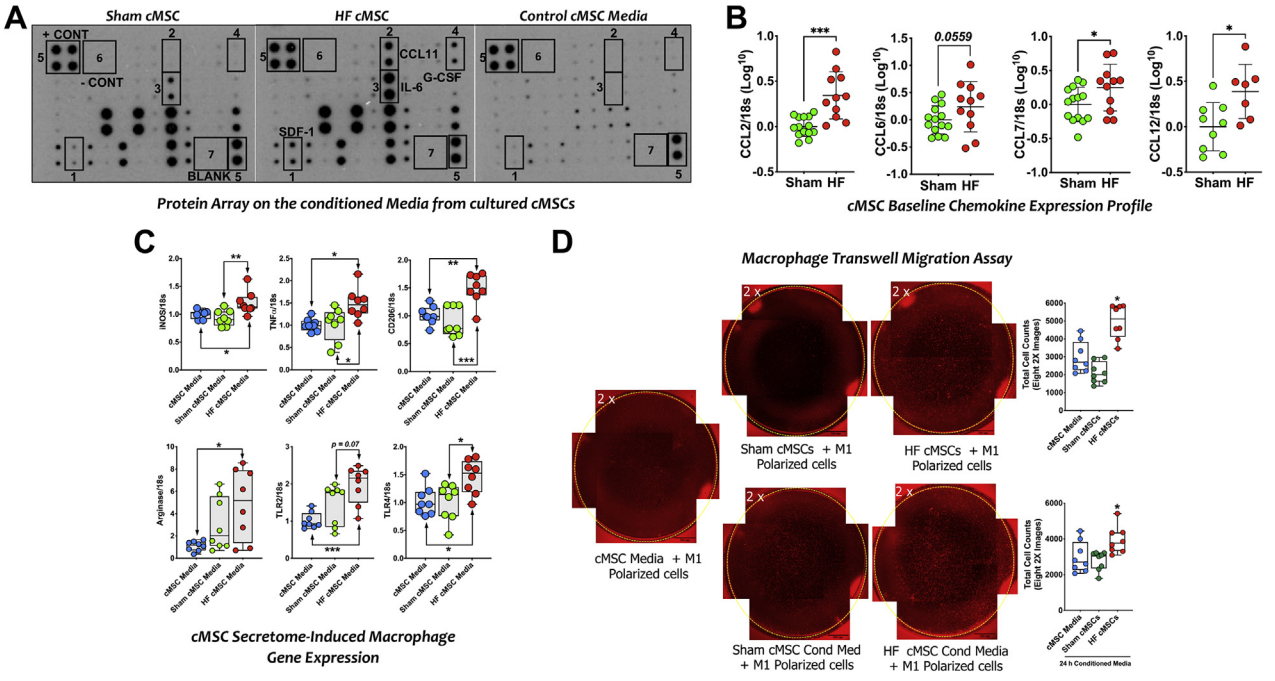

(A) Cell-free conditioned media from untreated sham and HF cMSCs cultured for 24 hours was analyzed for chemokine content using antibody arrays. cMSC media was used as control. Array controls (positive and negative), blanks, and some of the most dramatically up-regulated chemokines are indicated by **numbered boxes**. **(B)** Quantitative polymerase chain reaction analysis of baseline gene expression from sham and HF cMSCs for genes involved in monocyte and T-cell recruitment. Data are represented as mean ± SD of 3 to 4 independent experiments done in duplicate or triplicate. Statistical comparisons (unpaired Student's t-test) in **B** were performed after logarithmic data transformation to satisfy the normality assumption as described in the Methods. *$P < 0.05$, ***$P < 0.005$. **(C)** Quantitative polymerase chain reaction analysis of genes involved in macrophage polarization after 24 hours of co-culture of mouse RAW246.7 macrophage cells and conditioned media collected from untreated sham and HF cMSCs. Results are expressed as mean ± SD of 3 independent experiments done in duplicate or triplicate. *$P < 0.05$, **$P < 0.005$. **(D)** Results from Transwell migration assay showing representative images and the group data of the migrated M1-polarized mouse RAW 246.7macrophages when co-cultured with either sham or HF cMSCs **(upper panel)** or the conditioned (Cond) media collected from untreated sham and HF cMSCs **(lower panel)** as chemoattractant in the bottom wells of the Transwell plates. cMSC media was used as control. Each image is a stitched composite of 4 separate overlapping images. The **yellow dotted circle** demarcates the boundary of the Transwell. Four independent areas of observation were counted from each Transwell. Data are expressed mean ± SD of 2 independent experiments with multiple replicates. *$P < 0.05$ vs sham groups and control cMSC media. Statistical comparisons in **C and D** were analyzed by 1-way analysis of variance followed by Tukey's post hoc analysis. CCL = C-C motif chemokine ligand; G-CSF = granulocyte-colony stimulating factor; IL-6 = interleukin-6; iNOS = inducible nitric oxide synthase; SDF-1 = stromal cell-derived factor 1; TNF = tumor necrosis factor; TLR = Toll-like receptor; other abbreviations as in Figures 1 and 2.

(Figure 3D), findings that were recapitulated by HF cMSC-conditioned media (24 hours) in place of HF cMSCs as the chemoattractant stimulus.

Transcriptional profiling was performed on flow-sorted primary $CD45^{-}Sca1^{+}$ cells from sham-operated and HF hearts (8 weeks' post-MI) by using RNA-sequencing analysis. As illustrated in Figure 4A, $CD45^{-}Sca1^{+}$ cells from failing hearts exhibited marked alterations of their transcriptomic profile, with ~400 differentially expressed genes compared with sham $CD45^{-}Sca1^{+}$ cells. Ingenuity Pathway Analysis of differentially expressed genes supported a pro-fibrotic and pro-inflammatory phenotype of HF cMSCs with greater predicted activation of transforming growth factor-β (TGFβ), IL-6, and nuclear factor-κB signaling pathways (Figure 4B). Collectively, these data suggest that cMSCs undergo a phenotypic switch in the failing heart milieu that promotes tissue fibrosis and inflammation, and facilitates the infiltration and activation of pro-inflammatory macrophages.

MACROPHAGES PROMOTE MYOFIBROBLAST DIFFERENTIATION OF cMSCs IN THE FAILING HEART. The failing heart is characterized by both expanded tissue macrophages and fibrosis.[2] Hence, we evaluated whether macrophages modulate myofibroblast differentiation of cMSCs. TGFβ-induced myofibroblast differentiation was confirmed in naive

FIGURE 4 HF-Derived cMSCs Exhibit a Pro-fibrotic and Pro-inflammatory Phenotype

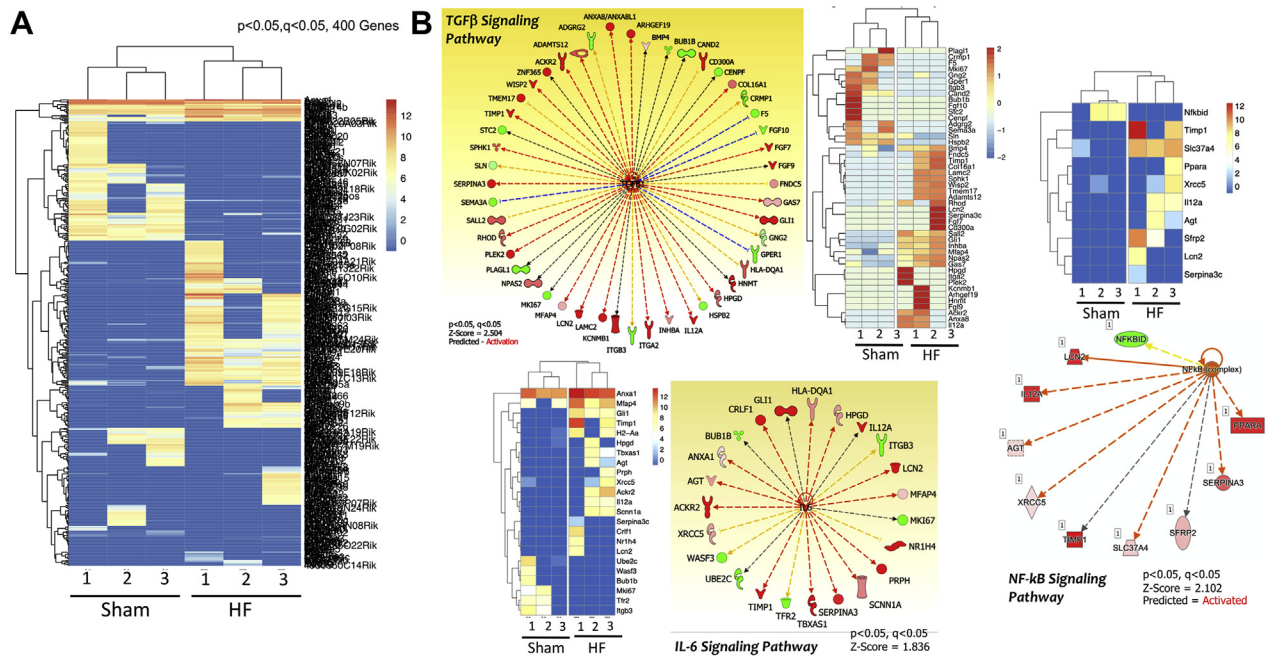

(A) Hierarchical clustering and heat maps of RNA-sequencing data from CD45$^-$Sca1$^+$ flow sorted from myocardial mononuclear cell isolates from sham and HF hearts (8 weeks' post-MI; n = 3 per group). Counts were normalized with DeSeq2 and then transformed via log 2 before clustering and visualization using the R platform. Shown is the data set generated using both $P < 0.05$ and $q < 0.05$ values (adjusted P value using false discovery rate value <0.05). **(B)** Upstream regulator analysis of genes identified from RNA-sequencing data (data obtained with $P < 0.05$ and $q < 0.05$ cutoffs; 400 genes) using Ingenuity Pathway Analysis software predicted among other pathway, activation of the pro-fibrotic transforming growth factor-β (TGFβ) pathway, and inflammatory pathways including IL-6 and nuclear factor-κB (NF-κB) signaling pathway. Abbreviations as in Figures 1 to 3.

cMSCs by α-SMA gene expression, immunostaining, and immunoblotting (Figure 5A). Collagen gel contraction assays revealed comparable TGFβ-induced myofibroblast differentiation (indexed by collagen gel contraction) of both sham and HF cMSCs (Figure 5B); nonetheless, gene expression of fibrotic markers collagen-I, collagen-III, and fibronectin, and the myofibroblast marker α-SMA, was augmented ~3- to 7-fold in TGFβ-differentiated HF cMSCs vs sham cMSCs (Figure 5C).

We next co-cultured naive RAW 264.7 macrophages with either sham or HF cMSCs in collagen gels. As shown in Figure 5D, macrophage co-culture robustly increased the myofibroblastic phenotype of HF cMSCs but not sham cMSCs. Macrophages were subsequently polarized in vitro to an M1 or an M2 phenotype before co-culture with either cMSCs or National Institutes of Health 3T3 fibroblasts (ATCC CRL-1658) in collagen gels. As illustrated in Figure 5E, M2 macrophages (but not M1 macrophages) induced myofibroblast differentiation of 3T3 fibroblasts. In contrast, both M1 and M2 macrophages induced myofibroblast differentiation of HF cMSCs, with a much more marked contraction response to M1 macrophages, whereas neither induced myofibroblasts from sham cMSCs. These results were recapitulated by substitution of macrophage-conditioned media in place of macrophages for the gel contraction studies (data not shown). Together, these results indicate that pro-inflammatory macrophages induce profound, and perhaps inappropriate, differentiation of HF-derived cMSCs into functional myofibroblasts, and suggest that a macrophage-cMSC interaction can drive fibrosis in the failing heart.

HF cMSCs INCREASE PDGFRβ EXPRESSION. PDGFR activation enhances fibroblast proliferation and collagen synthesis.[37] We measured baseline expression of the 2 PDGFR isoforms in cMSCs. As seen in Figure 6A, sham cMSCs exhibited predominant PDGFRα expression (~4-fold higher than HF cMSCs), whereas HF cMSCs exhibited predominant PDGFRβ expression (~3-fold higher than sham cMSCs). The switch in PDGFR expression from alpha to beta in HF cMSCs was additionally validated by immunoblot

FIGURE 5 cMSC-Macrophage Interactions Induce cMSC Myofibroblast Differentiation

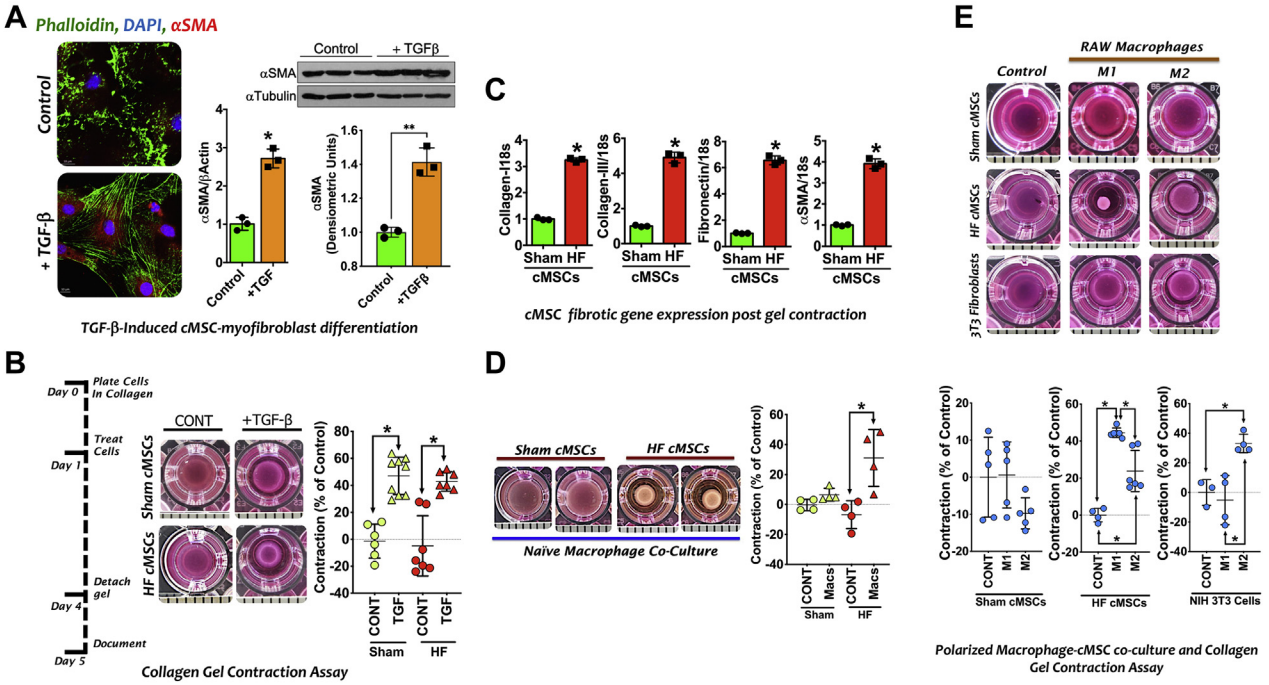

(A) Overlaid confocal images **(left)** of sham cMSCs treated with TGFβ (10 ng/mL) for 4 days and immunostained for α-SMA **(red)**, phalloidin **(green)**, and 4′,6-diamidino-2-phenylindole (DAPI) **(blue)**. **Middle:** quantitative polymerase chain reaction analysis and protein immunoblotting of α-SMA expression in TGFβ-differentiated (and control undifferentiated) sham cMSCs. n = 3 per group. **(B)** Functional assessment of TGFβ-induced myofibroblast differentiation of sham and HF cMSCs using collagen gel contraction assay and the corresponding quantification. Data are expressed as percent change in the collagen gel area relative to the area of the culture well. **(C)** Quantitative polymerase chain reaction analysis of fibrotic gene markers in TGFβ-differentiated sham and HF cMSCs isolated from collagen gels by collagenase digestion after contraction assay. n = 2 per group (each pooled from 2 independent wells) run in triplicates. **(D)** Representative results of collagen gel contraction assay from naive macrophage (mouse RAW 246.7 macrophages) with either sham or HF cMSC co-culture and the corresponding quantification. Results obtained from sham and HF cMSCs cultured with RAW-macrophages were used as control. n = 4 per group. **(E)** Results from M1- and M2-polarized mouse RAW 246.7 macrophage co-culture on myofibroblast differentiation of sham and HF cMSCs, and National Institutes of Health 3T3 fibroblasts with the corresponding quantification of collagen gel contraction. Results in **B and E** are representative of 2 to 4 independent experiments done in duplicate or triplicate. Data in **A and C** were analyzed by Student's *t*-test, and data in **B, D, and E** were analyzed by 1-way analysis of variance followed by Tukey's post hoc analysis. $*P < 0.05$, $**P < 0.005$. Other abbreviations as in Figures 1, 2, and 4.

analysis of PDGFR protein. HF cMSCs also exhibited increased baseline mRNA levels of the PDGFRβ ligands PDGF-B, and PDGF-D (Figure 6B). Notably, exposure to conditioned medium from M1-polarized RAW 264.7 macrophages increased HF cMSC expression of PDGF-A and PDGF-B, and exposure to either M1 or M2 macrophage-conditioned medium increased expression of PDGF-D, compared with sham cMSCs (Figure 6C).

The role of PDGFR in macrophage-facilitated differentiation of HF cMSCs to myofibroblasts was probed in collagen gel contraction assays by using the PDGFR inhibitor imatinib mesylate (10 μM). Co-culture of HF cMSCs with conditioned media from M1-polarized macrophages (but not M2-polarized macrophages) induced collagen gel contraction (Figure 6D). Imatinib treatment profoundly attenuated this response. Parallel experiments showed that a 4-day exposure to imatinib also significantly decreased α-SMA gene and protein expression in HF cMSCs. Identical collagen contraction gel responses were observed upon knockdown of PDGFRβ expression in HF cMSCs using PDGFRβ siRNA (30 nM) compared with control siRNA transfection, confirming specificity of the response. Notably, PDGFRβ siRNA-transfected HF cMSCs exhibited >95% loss of PDGFRβ protein expression over a period of 4 days. Collectively, these results support a key role for PDGF-PDGFRβ signaling in the fibrotic response linked to cMSCs and their interactions with macrophages.

IMATINIB TREATMENT IN VIVO ATTENUATES POST-MI LV REMODELING AND FIBROSIS. In view of the aforementioned results with isolated cMSCs, we

FIGURE 6 **HF cMSCs Exhibit Increased Expression of PDGFRβ That Promotes Their Myofibroblast Differentiation**

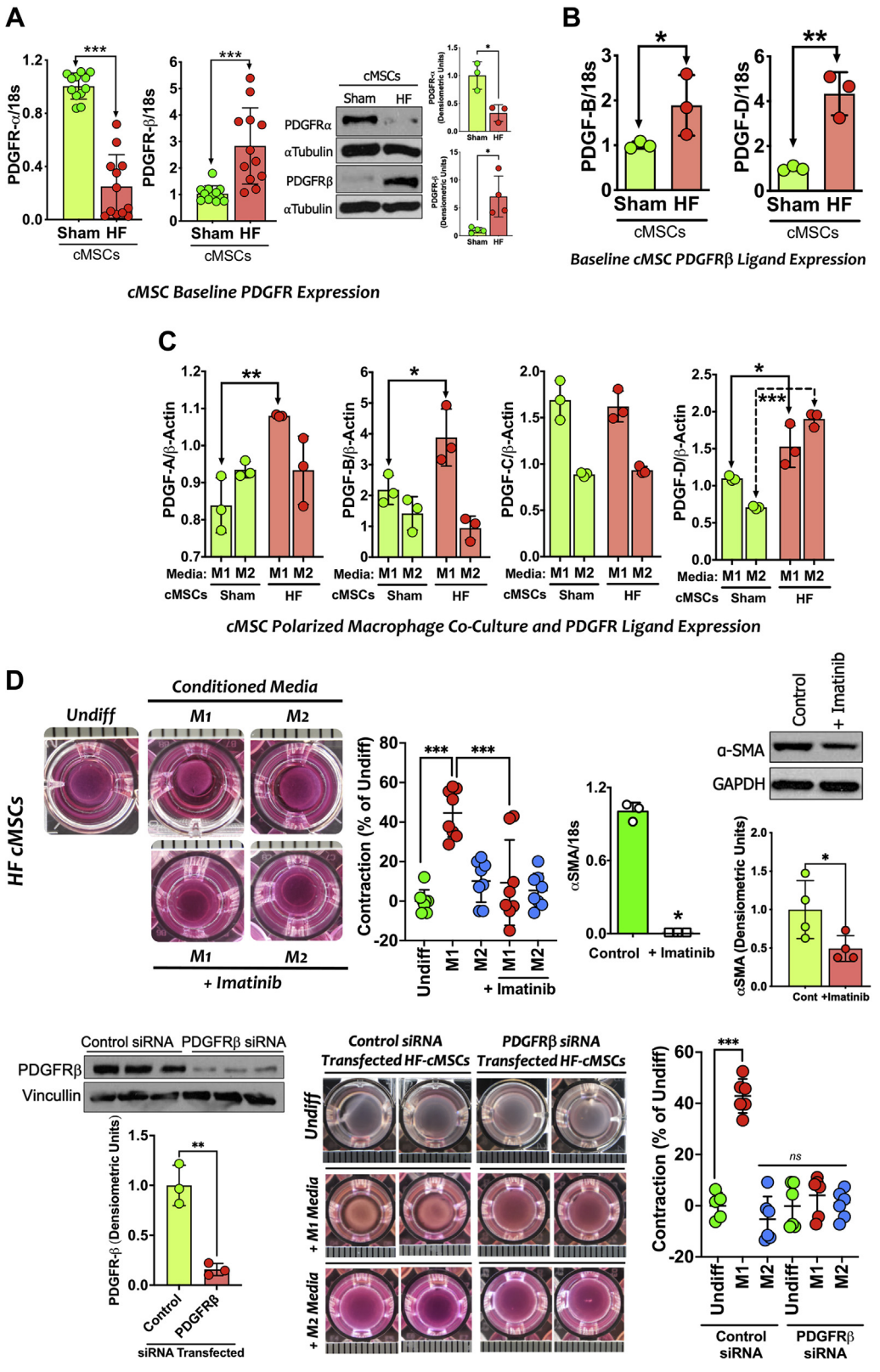

Continued on the next page

evaluated the in vivo effects of PDGFR inhibition on cardiac remodeling in the post-MI failing heart. To avoid suppression of essential early inflammation and wound healing, and to focus the evaluation on chronically remodeled hearts after nonreperfused MI, we administered either imatinib (30 mg/kg) or PBS vehicle intraperitoneally daily to mice from 2 to 5 weeks' post-MI, and to sham-operated control mice (Figure 7A). Echocardiography was performed at 2 weeks' post-MI to ensure comparable degrees of post-MI LV remodeling and dysfunction before treatment randomization.

As shown in Figures 7A and 7B, HF mice in both treatment groups had similar LV end-diastolic (EDV) and end-systolic volume (ESV) and EF before starting treatment. PBS-treated HF mice exhibited progressive LV dilatation (greater EDV and ESV) and systolic dysfunction (lower EF) over the treatment period. In contrast, imatinib-treated HF mice exhibited no further deterioration of LV size or function, indicating abrogation of LV remodeling. Analysis of changes in EDV, ESV, and EF revealed significantly smaller ΔEDV and ΔESV, and a trend toward smaller ΔEF, in imatinib-treated HF mice vs PBS-treated HF mice (Figure 7C). In contrast, in a parallel group of similarly treated sham-operated mice, neither imatinib nor vehicle affected LV size or systolic function over the 3-week treatment period (Supplemental Figure 3).

Gravimetric analysis (Figure 8A) revealed smaller normalized heart weight in imatinib-treated HF mice compared with PBS-treated HF mice, with no differences in normalized spleen or wet lung weights. Histologic assessment (Figure 8B, Supplemental Figure 4) revealed that imatinib-treated failing hearts exhibited significantly smaller cardiomyocyte area (~30% decrease), less border zone fibrosis (~60% decrease), and higher capillary density compared with PBS-treated hearts. There were no differences in remote zone fibrosis (data not shown). Flow cytometric evaluation revealed comparable levels of cardiac $CD45^{-}Sca1^{+}$ cMSCs, as well as total $CD45^{+}$ leukocytes, total $MerTK^{+}MHCII^{+}Ly6C^{-}F4/80^{+}$ macrophages, and $CCR2^{-}$ resident macrophages between the treatment groups (Figure 9). However, compared with PBS-treated HF mice, imatinib-treated HF mice exhibited significantly fewer $CCR2^{+}$ infiltrating macrophages in the heart. No differences in the abundance of either $CCR2^{+}$ or $CCR2^{-}$ macrophages were observed between sham-operated hearts treated with imatinib or PBS (Supplemental Figure 5). However, as expected, we observed ~9-fold higher ($P = 0.047$) total cardiac macrophages, ~152-fold higher ($P = 0.023$) $CCR2^{+}$ macrophages, and ~7.6-fold higher ($P = 0.054$) $CCR2^{-}$ macrophages in PBS-treated HF mice vs PBS-treated sham mice. Collectively, these data suggest that imatinib-mediated PDGFR inhibition alleviated the progression of chronic post-MI cardiac remodeling, inflammation, and fibrosis.

DISCUSSION

The current study uncovered a novel pro-fibrotic axis in HF mediated by alterations in the phenotype and function of resident cMSCs. There are several key findings. First, a distinct resident $Sca1^{+}CD31^{-}DDR2^{-}$ MSC population significantly expands and develops a pro-inflammatory and pro-fibrotic profile in the failing heart, potentially serving as an additional source of myofibroblasts. Second, mutual interactions between cMSCs and macrophages

FIGURE 6 Continued

(A) Platelet-derived growth factor receptor (PDGFR) expression in sham and HF cMSCs by quantitative polymerase chain reaction (qPCR) (left, n = 3-4 per group) and immunoblot analysis (right, n = 3-4 per group). Results are presented as mean ± SD. **(B)** qPCR analysis for baseline expression of PDGFRβ ligands PDGF-B and PDGF-D in sham and HF cMSCs. n = 3 per group. **(C)** qPCR analysis of PDGFR ligand expression in sham and HF cMSCs after 24 hours of co-culture with cell-free conditioned media collected from in vitro polarized mouse RAW 246.7 macrophages. n = 3 per group. **(D) Upper panel:** Representative results from collagen gel contraction assay and corresponding quantitation upon HF cMSCs co-culture with cell-free conditioned media from polarized macrophages (Raw 246.7 cells) for 4 days in the absence or presence of overnight treatment with 10 μM imatinib. Quantitation is from 4 independent experiments. Also shown are results from qPCR and immunoblot assays for α-SMA expression in HF cMSCs treated with imatinib for 4 days. n = 3 per group. *P* value comparison is vs control untreated cells. **Lower panel: Left,** Immunoblotting for PDGFRβ in HF cMSCs after 96 hours of transfection with PDGFRβ-specific (or control) small interfering RNA (siRNA) (30 nM). n = 3 per group. **Right:** Representative results from collagen gel contraction assays, and the corresponding quantification, using siRNA-transfected HF cMSCs and conditioned media from in vitro polarized RAW 246.7 macrophages. Quantitation reflects 2 independent experiments each done in triplicate. Data in **A, B, and D** (α-SMA and PDGFRβ data) were analyzed by using Student's *t*-test, and data in **C and D** (gel contraction data) were analyzed by 1-way analysis of variance followed by either Tukey's **(D)** or Šidák's **(C)** post hoc analysis. $*P < 0.05$, $**P < 0.005$, $***P < 0.001$. GAPDH = glyceraldehyde-3-phosphate dehydrogenase; other abbreviations as in Figures 1 and 2.

FIGURE 7 Imatinib Treatment Post-MI Attenuates LV Remodeling and Preserves Systolic Function

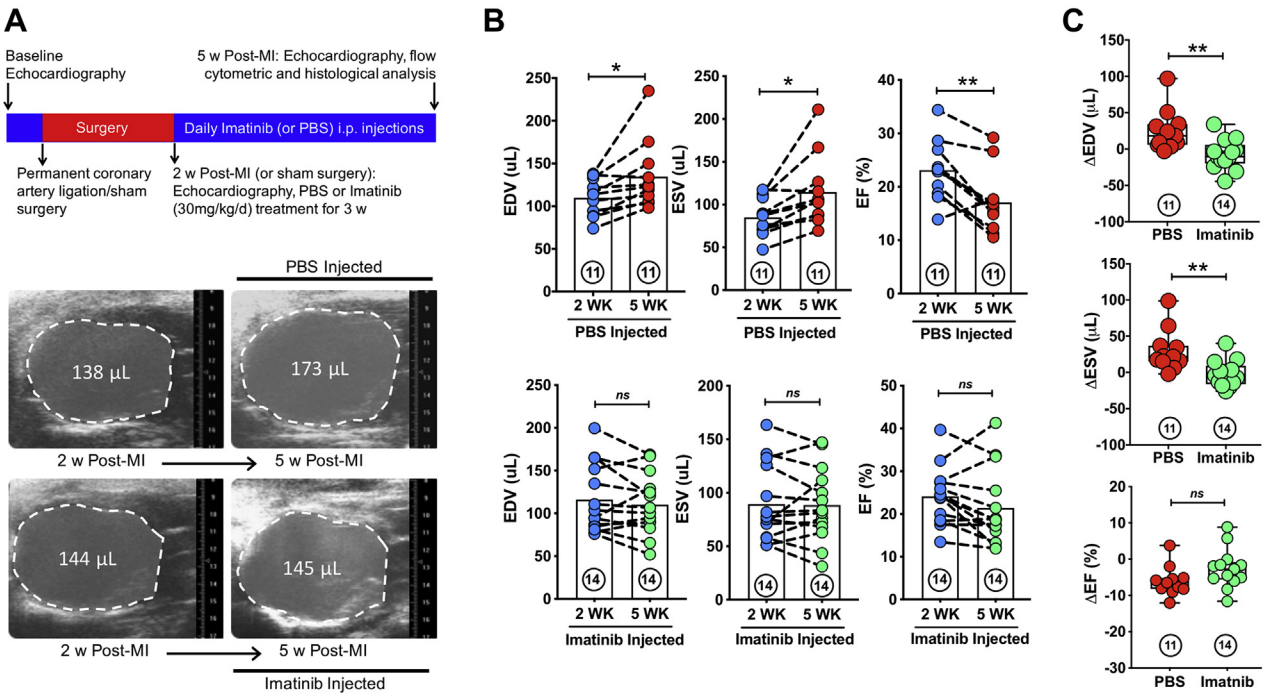

(A) Top: Schematic of the experiment protocol. Following 2 weeks of permanent coronary artery ligation (or sham surgery), wild-type C57BL/6 mice were randomized to receive daily injections of either 200 µL phosphate-buffered saline (PBS) vehicle or imatinib (30 mg/kg) for 3 weeks before being reassessed by echocardiography and subsequent euthanasia. **Bottom:** Representative long-axis B-mode serial echocardiographic images at end-diastole from HF mice at 2 and 5 weeks' post-MI after treatment with either PBS or imatinib as described in **A**. The dotted line marks the left ventricular (LV) cavity. **(B)** Corresponding paired echocardiographic group data from HF mice at 2 and 5 weeks' post-MI after treatment with either PBS or imatinib as described in **A**. n = 11 to 14 per group. **(C)** Echocardiographic group data depicting changes (Δ) in end-diastolic volume (EDV) and end-systolic volume (ESV) and ejection fraction (EF) from 2 to 5 weeks' post-MI with treatment with either PBS or imatinib as described in **A**. n = 11 to 14 per group. Data were analyzed by using either paired **(B)** or unpaired **(C)** Student's *t*-test. $*P < 0.05$, $**P < 0.005$. Abbreviations as in Figures 1 to 4.

promote pro-fibrotic and pro-inflammatory effects, such that HF cMSCs polarize and attract activated macrophages, whereas M1 macrophages induce myofibroblast differentiation of HF cMSCs. Third, PDGF-PDGFR signaling contributes importantly to the pro-fibrotic and pro-inflammatory responses of cMSCs in HF, likely related in large part to PDGFRβ activation, as this PDGF isoform, and its corresponding ligands, were differentially up-regulated in cMSCs from failing hearts. Fourth, receptor tyrosine kinase inhibition with imatinib inhibited macrophage-induced cMSC myofibroblast differentiation and improved LV fibrosis, function, remodeling, and monocyte-derived macrophage infiltration in vivo during post-MI HF, underscoring a potential approach to clinical translation. Hence, cMSCs in the failing heart channel a maladaptive myofibroblastic and pro-inflammatory fate, and this phenotypic switch is sustained, at least in part, by tissue macrophages and PDGFR signaling. Conceptually, our findings suggest that restoring or maintaining a normal cMSC phenotype may represent a novel approach for combating pathologic fibrosis in the failing heart. Given that the PDGFR inhibitor imatinib is clinically approved for human use,[38,39] our studies provide rationale for testing this drug as a primary therapeutic in HF.

Multiple studies have characterized stem cells from mouse hearts based on surface markers. We isolated cMSCs based on selective depletion of Lin^+ hematopoietic cells, $CD31^+$endothelial cells, and $DDR2^+$ fibroblasts, and enrichment of Sca1-expressing cells. Cells derived with this approach robustly expressed MSC markers such as CD90 but lacked fibroblast and myofibroblast markers, and did not exhibit surface c-Kit expression. Importantly, however, upon appropriate stimulation, cMSCs were

FIGURE 8 Imatinib Treatment Post-MI Decreases Myocardial Fibrosis and Cardiomyocyte Hypertrophy and Enhances Myocardial Capillary Density

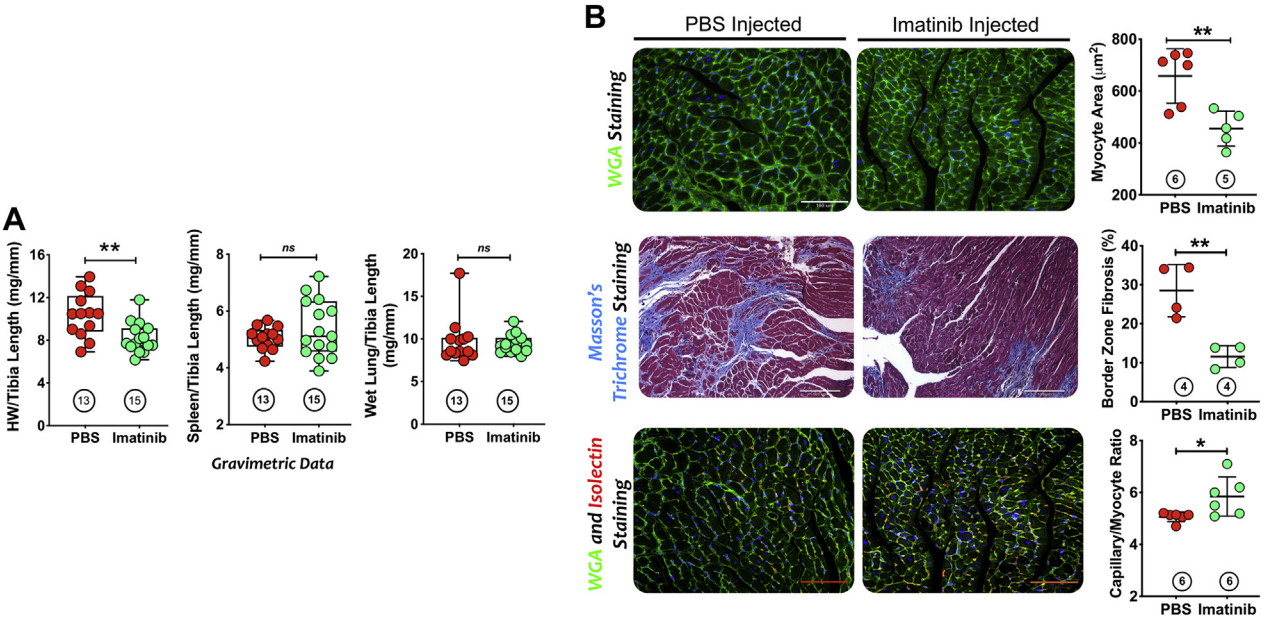

(A) LV mass/tibia length ratio from wild-type HF mice at 5 weeks after treatment with either 200 μL PBS or imatinib (30 mg/kg per day) for 3 weeks starting 2 weeks after MI. n = 13 to 15 per group. **(B)** Representative wheat germ agglutinin (WGA) **(green)** and 4′,6-diamidino-2-phenylindole **(blue)** overlaid staining of the left ventricle and quantification of cardiomyocyte hypertrophy (**upper panel**, **top**; scale bar = 100 μm), Masson's trichrome stains and quantification of LV border zone fibrosis **(middle panel)**, and cardiac isolectin **(red)**, WGA **(green)**, and 4′,6-diamidino-2-phenylindole **(blue)** stained and combined images and corresponding quantification of capillary:cardiomyocyte ratio in remote zone left ventricle from HF mice after treatment with either PBS or imatinib at 2 weeks' post-MI **(bottom panel)**. n = 4 to 6 per group. Data in **A and B** were analyzed by using unpaired Student's *t*-test. Scale bars = 100 μm. *$P < 0.05$, **$P < 0.005$. HW = heart weight; other abbreviations as in Figures 1, 2, and 7.

capable of differentiation in vitro to broader mesodermal (adipogenic, osteogenic, and chondrogenic) lineages as well as to myofibroblasts. Hence, Sca1$^+$ cMSCs represent a resident cMSC population distinct from MSC-like cardiosphere-derived cells that grow as self-assembling clusters in suspension cultures, and exhibit low c-Kit and varying CD90 expression, both of which negatively correlate with therapeutic benefits induced by cardiosphere-derived cells.[40]

cMSCs are significantly expanded in chronically remodeled failing hearts post-MI (eg, ischemic cardiomyopathy) and exhibit a pathologic pro-fibrotic and pro-inflammatory profile at transcriptional, translational, and functional levels. Indeed, whereas (Sca1$^-$) DDR2$^+$ fibroblasts[41] expanded acutely after MI, consistent with their indispensable role in post-MI wound healing and scar formation,[42] these cells, surprisingly, were not increased in the chronically failing heart. In contrast, Sca1$^+$CD31$^-$DDR2$^-$ cMSCs were not increased acutely after MI but were robustly expanded ~6-fold in chronic HF and accompanied by a nearly 20-fold increase in α-SMA$^+$DDR2$^-$Sca1$^+$ myofibroblasts. Moreover, the transcriptomic profile of primary sorted cMSCs in HF indicated heightened pro-fibrotic TGF-β pathway activation. These results suggest that phenotypically altered cMSCs are important contributors to pathologic fibrosis in the chronically failing heart. However, given the overlap of surface markers between MSCs, fibroblasts, and pericytes, more extensive transcriptomic and proteomic studies of cMSCs will be needed to definitively establish their biological properties.

Our observations regarding cMSCs are consistent with prior studies establishing that perivascular[12] and epicardial[43] MSC-like cells in the heart are important cellular sources of myofibroblasts and organ fibrosis in nonischemic and ischemic models of cardiac injury, respectively. Although fibroblasts are considered the main effector cells of cardiac fibrosis, the role of chronic fibroblast activation in the pathogenesis of ischemic cardiomyopathy is unknown.[44] Our data suggest differential roles for cardiac fibroblasts and

FIGURE 9 Imatinib Treatment Attenuates Post-MI Myocardial Inflammation

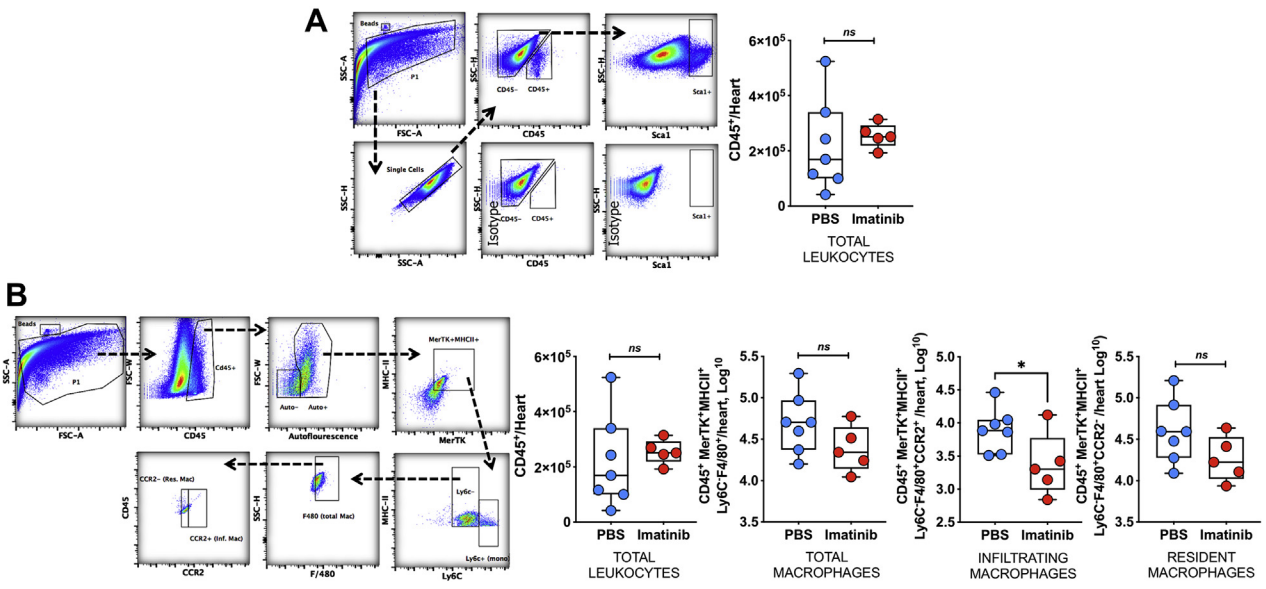

(A) Representative flow cytometry scatter plots and corresponding group quantification of cMSCs ($CD45^-Sca1^+$) in HF hearts after treatment with either PBS or imatinib (30 mg/kg per day) for 3 weeks after 2 weeks of MI. **(B)** Representative flow cytometry gating strategy and quantitation of total leukocytes ($CD45^+$), total macrophages ($CD45^+MerTK^+MHCII^+Ly6C^-F4/80^+$), infiltrating macrophages ($CD45^+MerTK^+MHCII^+Ly6C^-F4/80^+CCR2^+$), and resident macrophages ($CD45^+MerTK^+MHCII^+Ly6C^-F4/80^+CCR2^-$) from experimental groups as in **panel A**. n = 4 to 7 per group. Data in **A and B** were analyzed by using unpaired Student's *t*-test (statistical comparisons in **B** were performed after logarithmic data transformation to satisfy the normality assumption as described in the Methods). Data are presented as cells per heart. *$P < 0.05$. FSC-A = forward scatter–area; FSC-W = forward scatter–width; MHC-II = major histocompatibility complex-II; SSC-A = side scatter–area; other abbreviations as in Figures 1 to 4 and 7.

cMSCs as effectors of fibrosis during post-MI cardiac remodeling, with cardiac fibroblasts as drivers of wound healing and scar formation in the acute and subacute stages, and cMSCs as mediators of pathologic fibrosis during chronic remodeling and failure.

Tissue fibrosis in chronic diseases such as HF is closely interlinked with inflammation and immune cell activation.[1,13] MSCs are well known to be broadly immunoregulatory, with the capacity to either suppress or promote immune responses in response to the microenvironment.[45,46] A key finding of our study is that in addition to pro-fibrotic features, cMSCs from the failing heart are distinctly pro-inflammatory and harbor a reciprocal relationship with M1-type macrophages that may further amplify fibrotic and inflammatory tissue responses. At the transcript level, HF cMSCs displayed activation of IL-6- and nuclear factor-κB-linked inflammatory pathways, and up-regulation of multiple chemokines, including CCL2, CCL7, and CCL12, the ligands for CCR2, a key marker of monocyte-derived tissue-infiltrating macrophages in the heart.[47] Moreover, the HF cMSC secretome was sufficient to induce both polarization of naive macrophages and chemotaxis of M1-type macrophages. In turn, macrophages, especially M1 macrophages, selectively induced myofibroblast differentiation of HF cMSCs (but not sham cMSCs). Given that HF is characterized by pro-inflammatory cardiac macrophage expansion,[1] this suggests a feed-forward mechanism promoting tissue fibrosis involving a macrophage-cMSC interaction in the failing heart. We propose that cMSCs in failing hearts lose immunomodulatory properties, which then serves to trigger and sustain chronic inflammation and fibrosis.

The PDGF signaling axis is an important stimulator of fibrosis in various organ pathologies, including those of the heart,[15-17,48] and hence we explored its potential role in altering the cMSC phenotype in HF. PDGF signals via 2 transmembrane tyrosine kinases receptors, PDGFRα and PDGFRβ.[49] Whereas PDGFRα has been proposed as an MSC marker,[50] the role of PDGFRβ in MSCs is poorly defined. We found that failing heart cMSCs switch from predominant PDGFRα to PDGFRβ expression, and up-regulate their corresponding ligands PDGF-B and PDGF-D. Moreover,

JACC: BASIC TO TRANSLATIONAL SCIENCE VOL. 7, NO. 5, 2022
MAY 2022:465–483

PDGFRβ ligand expression further augments upon exposure to macrophages, especially M1 macrophages. Thus, with augmented cMSC-macrophage interactions occurring in the failing heart, cMSCs would constantly be exposed to a PDGF-rich microenvironment that sustains chronic PDGFRβ activation and subsequent downstream pro-fibrotic responses. Analogous inflammation-driven PDGFR expression switching has also been described in hepatic satellite cells in chronic liver fibrosis and airway fibroblasts in asthma.[51,52]

Imatinib is a potent inhibitor of the receptor tyrosine kinases Bcr-Abl (in human chronic myelogenous leukemia), PDGFRα and PDGFRβ, and c-kit.[53] We used imatinib to probe the functional role of PDGFRβ activation in the pro-fibrotic phenotype of cMSCs and cardiac remodeling in HF. In vivo administration of imatinib to mice with established cardiac remodeling and HF abrogated progression of LV dysfunction and improved remodeling at both the chamber and tissue level, including salutary effects on border zone fibrosis, capillary density, and $CCR2^{+}$ monocyte-derived macrophage infiltration. In vitro, imatinib markedly attenuated macrophage-induced myofibroblast differentiation of HF cMSCs, which may partly underlie its beneficial in vivo impact on myocardial fibrosis and function. As noted earlier, imatinib was given systemically and is not a specific inhibitor of PDGFRβ. Therefore, the observed beneficial effects of imatinib may not be solely caused by effects on cMSCs, and this must be acknowledged as a study limitation. Nonetheless, although imatinib is not a selective PDGFR inhibitor, these results are wholly consistent with a meaningful and important effect on cMSC-localized inactivation of PDGF-β signaling. PDGFRs are primarily localized to interstitial and vascular cells in the heart,[54] with age-dependent cardiomyocyte PDGFRβ inactivation starting by 2 weeks following birth.[55] Our FACS analysis further indicated that $Sca1^{+}$ cMSCs rather than $DDR2^{+}$ fibroblasts are the primary mesenchymal cell type expanded and sourcing myofibroblasts in the failing heart, and that these cMSCs exhibit PDGF-β signaling predominance. Finally, we observed no c-Kit expression in cardiac mesenchymal cells. Hence, our results strongly suggest that altered cMSC PDGF signaling plays a key role in sustaining the pro-fibrotic and inflammatory responses observed in the failing heart, and that inhibiting this axis may represent a potential therapeutic approach for reducing cardiac fibrosis and inflammation in HF.

Our findings with imatinib in chronic LV remodeling and failure extend prior studies showing imatinib-mediated improvements in cardiac fibrosis in murine models of reperfused MI, β-adrenergic activation, and myocarditis.[19-21] Notably, however, the salutary effects of imatinib early after reperfused MI seem related to PDGFRα inactivation, as specific antibody-mediated PDGFRβ inhibition led to impaired scar and vasculature maturation, and prolonged inflammation.[21] In humans, imatinib has been suggested to be cardiotoxic.[56] However, several subsequent clinical studies of imatinib-treated patients have reported a low incidence of cardiac dysfunction comparable to the expected population incidence.[57,58] Importantly, the imatinib dose we used was substantially lower than the dose used for leukemia treatment in humans, as determined by a dose-conversion formula,[26] suggesting that low doses which avoid imatinib toxicity in humans may be considered in HF. Obviously, this concept would need to be tested and validated in clinical studies.

Our results also have implications for cMSC-based cell therapy to affect cardiac repair. MSCs have been considered an ideal stem cell type for regenerative therapy in view of their immunomodulatory properties.[59] To date, however, autologous transplantation of MSCs (and other stem cell types) in HF has had very limited clinical success,[60,61] whereas animal models have reported low cell survival, myocardial engraftment, and persistence.[62-64] Our results suggest that an important factor limiting cMSC therapy may be a cardiac microenvironment that pathologically channels cMSCs away from immunomodulation and toward fibrosis and inflammation, thus severely limiting benefit. Although not directly tested, our results further support the idea that PDGFR inhibition at the time of cMSC delivery and the peri-transplantation period may be a fruitful adjunctive approach to improve therapeutic efficacy.

CONCLUSIONS

We have shown that a cardiac resident $Sca1^{+}CD31^{-}DDR2^{-}$ MSC population, which does not exhibit fibroblast or myofibroblast characteristics at baseline, significantly expands and contributes to myofibroblast abundance in the failing heart and exhibits a pro-inflammatory and pro-fibrotic profile. Mutual cell-to-cell interactions between cMSCs and

macrophages, especially pro-inflammatory macrophages, promote and amplify the pro-fibrotic and pro-inflammatory responses in HF. Activated PDGF-PDGFR signaling, and a pathologic isoform switch to PDGF-β expression in cMSCs, plays a key role in the altered cMSC phenotype. Pharmacologic PDGFR inhibition robustly improves macrophage-induced cMSC myofibroblast differentiation, and LV fibrosis, function, inflammation, and remodeling in established HF post-MI HF, highlighting a potential approach for restoring normal cMSC phenotype as a primary therapeutic in HF.

ACKNOWLEDGMENT The authors thank Dr Suresh Verma at the University of Alabama at Birmingham (UAB) for providing adult mouse cardiac fibroblast RNA samples.

FUNDING SUPPORT AND AUTHOR DISCLOSURES

This work was supported by National Institutes of Health grants R01HL137046 (Dr Hamid) and R01HL125735 (Dr Prabhu), a VA Merit Award 101BX002706 (Dr Prabhu), and a pilot grant from the UAB Comprehensive Cardiovascular Center (Dr Hamid). The authors have reported that they have no relationships relevant to the contents of this paper to disclose.

ADDRESS FOR CORRESPONDENCE: Dr Tariq Hamid, Division of Cardiology, Washington University School of Medicine, 4565 McKinley Avenue, McDonnell Medical Sciences Building-751C, St. Louis, Missouri 63110, USA. E-mail: tariq@wustl.edu. OR Dr Sumanth D. Prabhu, Division of Cardiology, Washington University School of Medicine, 660 South Euclid Avenue, CB 8086, St. Louis, Missouri 63110, USA. E-mail: prabhu@wustl.edu.

PERSPECTIVES

COMPETENCY IN MEDICAL KNOWLEDGE: HF is characterized by chronic inflammation and pathologic fibrosis that promote disease progression. Although activated fibroblasts are classically considered primary mediators of fibrosis, to date strategies aimed at modulating fibroblast activation in HF have yet to translate to clinical practice. Our studies establish that resident cMSCs expand and exhibit pro-inflammatory and pro-fibrotic characteristics in HF, suggesting that along with fibroblasts, cMSCs contribute meaningfully to cardiac fibrosis. Furthermore, interaction between cMSCs and pro-inflammatory macrophages, which are also expanded in failing hearts, augments their pro-fibrotic fate and thereby may contribute to pathologic remodeling and fibrosis in HF. Attenuation of cMSC expansion or modulation of the myocardial pro-inflammatory microenvironment in HF may therefore be feasible approaches to prevent progressive remodeling and failure.

TRANSLATIONAL OUTLOOK: For clinical translation, these observations in mice should be confirmed in large animal models. These studies uncover a novel pro-fibrotic axis in HF related to enhanced PDGFRβ activation in cMSCs. PDGFRβ activation limits the immunomodulatory properties of cMSCs and channels a myofibroblast differentiation fate that promotes fibrotic and inflammatory responses. Restoring or maintaining a normal cMSC phenotype in HF may thus represent a promising therapeutic approach for reducing fibrosis and inflammation. Indirectly, our studies also suggest that circumscribed pharmacologic PDFR inhibition at the time of exogenous cMSC cell transplantation could be an effective strategy to improve the therapeutic efficacy of cMSC-mediated cardiac repair.

REFERENCES

1. Adamo L, Rocha-Resende C, Prabhu SD, Mann DL. Reappraising the role of inflammation in heart failure. *Nat Rev Cardiol*. 2020;17:269–285.

2. Ismahil MA, Hamid T, Bansal SS, Patel B, Kingery JR, Prabhu SD. Remodeling of the mononuclear phagocyte network underlies chronic inflammation and disease progression in heart failure: critical importance of the cardiosplenic axis. *Circ Res*. 2014;114:266–282.

3. Gabbiani G. The myofibroblast in wound healing and fibrocontractive diseases. *J Pathol*. 2003;200:500–503.

4. Tomasek JJ, Gabbiani G, Hinz B, Chaponnier C, Brown RA. Myofibroblasts and mechano-regulation of connective tissue remodeling. *Nat Rev Mol Cell Biol*. 2002;3:349–363.

5. Conrad CH, Brooks WW, Hayes JA, Sen S, Robinson KG, Bing OH. Myocardial fibrosis and stiffness with hypertrophy and heart failure in the spontaneously hypertensive rat. *Circulation*. 1995;91:161–170.

6. Burlew BS, Weber KT. Cardiac fibrosis as a cause of diastolic dysfunction. *Herz*. 2002;27:92–98.

7. Krenning G, Zeisberg EM, Kalluri R. The origin of fibroblasts and mechanism of cardiac fibrosis. *J Cell Physiol*. 2010;225:631–637.

8. Fan D, Takawale A, Lee J, Kassiri Z. Cardiac fibroblasts, fibrosis and extracellular matrix remodeling in heart disease. *Fibrogenesis Tissue Repair*. 2012;5:15.

9. Chong JJ, Chandrakanthan V, Xaymardan M, et al. Adult cardiac-resident MSC-like stem cells with a proepicardial origin. *Cell Stem Cell*. 2011;9:527–540.

10. Oldershaw R, Owens WA, Sutherland R, et al. Human cardiac-mesenchymal stem cell-like cells, a novel cell population with therapeutic potential. *Stem Cells Dev*. 2019;28:593–607.

11. Carlson S, Trial J, Soeller C, Entman ML. Cardiac mesenchymal stem cells contribute to scar formation after myocardial infarction. *Cardiovasc Res*. 2011;91:99–107.

12. Kramann R, Schneider RK, DiRocco DP, et al. Perivascular Gli1+ progenitors are key contributors to injury-induced organ fibrosis. *Cell Stem Cell*. 2015;16:51–66.

13. Prabhu SD, Frangogiannis NG. The biological basis for cardiac repair after myocardial infarction: from inflammation to fibrosis. *Circ Res*. 2016;119:91–112.

14. Andrae J, Gallini R, Betsholtz C. Role of platelet-derived growth factors in physiology and medicine. *Genes Dev*. 2008;22:1276–1312.

15. Klinkhammer BM, Floege J, Boor P. PDGF in organ fibrosis. *Mol Aspects Med*. 2018;62:44–62.

16. Ponten A, Li X, Thoren P, et al. Transgenic overexpression of platelet-derived growth factor-C in the mouse heart induces cardiac fibrosis, hypertrophy, and dilated cardiomyopathy. *Am J Pathol*. 2003;163:673–682.

17. Ponten A, Folestad EB, Pietras K, Eriksson U. Platelet-derived growth factor D induces cardiac fibrosis and proliferation of vascular smooth muscle cells in heart-specific transgenic mice. *Circ Res*. 2005;97:1036–1045.

18. Tuuminen R, Nykanen A, Keranen MA, et al. The effect of platelet-derived growth factor ligands in rat cardiac allograft vasculopathy and fibrosis. *Transplant Proc*. 2006;38:3271–3273.

19. Leipner C, Grun K, Muller A, et al. Imatinib mesylate attenuates fibrosis in coxsackievirus b3-induced chronic myocarditis. *Cardiovasc Res*. 2008;79:118–126.

20. Wang LX, Yang X, Yue Y, et al. Imatinib attenuates cardiac fibrosis by inhibiting platelet-derived growth factor receptors activation in isoproterenol induced model. *PLoS One*. 2017;12:e0178619.

21. Zymek P, Bujak M, Chatila K, et al. The role of platelet-derived growth factor signaling in healing myocardial infarcts. *J Am Coll Cardiol*. 2006;48:2315–2323.

22. Hamid T, Gu Y, Ortines RV, et al. Divergent tumor necrosis factor receptor-related remodeling responses in heart failure: role of nuclear factor-kappaB and inflammatory activation. *Circulation*. 2009;119:1386–1397.

23. Hamid T, Guo SZ, Kingery JR, Xiang X, Dawn B, Prabhu SD. Cardiomyocyte NF-kappaB p65 promotes adverse remodeling, apoptosis, and endoplasmic reticulum stress in heart failure. *Cardiovasc Res*. 2011;89:129–138.

24. Bansal SS, Ismahil MA, Goel M, et al. Dysfunctional and proinflammatory regulatory T-lymphocytes are essential for adverse cardiac remodeling in ischemic cardiomyopathy. *Circulation*. 2019;139:206–221.

25. Jang SW, Ihm SH, Choo EH, et al. Imatinib mesylate attenuates myocardial remodeling through inhibition of platelet-derived growth factor and transforming growth factor activation in a rat model of hypertension. *Hypertension*. 2014;63:1228–1234.

26. Reagan-Shaw S, Nihal M, Ahmad N. Dose translation from animal to human studies revisited. *FASEB J*. 2008;22:659–661.

27. Bansal SS, Ismahil MA, Goel M, et al. Activated T lymphocytes are essential drivers of pathological remodeling in ischemic heart failure. *Circ Heart Fail*. 2017;10:e003688.

28. Hamid T, Xu Y, Ismahil MA, et al. TNF receptor signaling inhibits cardiomyogenic differentiation of cardiac stem cells and promotes a neuroadrenergic-like fate. *Am J Physiol Heart Circ Physiol*. 2016;311:H1189–H1201.

29. Dominici M, Le Blanc K, Mueller I, et al. Minimal criteria for defining multipotent mesenchymal stromal cells. The International Society for Cellular Therapy position statement. *Cytotherapy*. 2006;8:315–317.

30. Dobin A, Davis CA, Schlesinger F, et al. STAR: ultrafast universal RNA-seq aligner. *Bioinformatics*. 2013;29:15–21.

31. Trapnell C, Roberts A, Goff L, et al. Differential gene and transcript expression analysis of RNA-seq experiments with TopHat and Cufflinks. *Nat Protoc*. 2012;7:562–578.

32. Trapnell C, Williams BA, Pertea G, et al. Transcript assembly and quantification by RNA-Seq reveals unannotated transcripts and isoform switching during cell differentiation. *Nat Biotechnol*. 2010;28:511–515.

33. Camelliti P, Borg TK, Kohl P. Structural and functional characterisation of cardiac fibroblasts. *Cardiovasc Res*. 2005;65:40–51.

34. Kishore R, Verma SK, Mackie AR, et al. Bone marrow progenitor cell therapy-mediated paracrine regulation of cardiac miRNA-155 modulates fibrotic response in diabetic hearts. *PLoS One*. 2013;8:e60161.

35. Souders CA, Bowers SL, Baudino TA. Cardiac fibroblast: the renaissance cell. *Circ Res*. 2009;105:1164–1176.

36. Trial J, Entman ML, Cieslik KA. Mesenchymal stem cell-derived inflammatory fibroblasts mediate interstitial fibrosis in the aging heart. *J Mol Cell Cardiol*. 2016;91:28–34.

37. Rajkumar VS, Shiwen X, Bostrom M, et al. Platelet-derived growth factor-beta receptor activation is essential for fibroblast and pericyte recruitment during cutaneous wound healing. *Am J Pathol*. 2006;169:2254–2265.

38. Distler JH, Manger B, Spriewald BM, Schett G, Distler O. Treatment of pulmonary fibrosis for twenty weeks with imatinib mesylate in a patient with mixed connective tissue disease. *Arthritis Rheum*. 2008;58:2538–2542.

39. Druker BJ, Tamura S, Buchdunger E, et al. Effects of a selective inhibitor of the Abl tyrosine kinase on the growth of Bcr-Abl positive cells. *Nat Med*. 1996;2:561–566.

40. Cheng K, Ibrahim A, Hensley MT, et al. Relative roles of CD90 and c-kit to the regenerative efficacy of cardiosphere-derived cells in humans and in a mouse model of myocardial infarction. *J Am Heart Assoc*. 2014;3:e001260.

41. Goldsmith EC, Hoffman A, Morales MO, et al. Organization of fibroblasts in the heart. *Dev Dyn*. 2004;230:787–794.

42. Daseke MJ 2nd, Tenkorang MAA, Chalise U, Konfrst SR, Lindsey ML. Cardiac fibroblast activation during myocardial infarction wound healing: fibroblast polarization after MI. *Matrix Biol*. 2020;91-92:109–116.

43. Ruiz-Villalba A, Simon AM, Pogontke C, et al. Interacting resident epicardium-derived fibroblasts and recruited bone marrow cells form myocardial infarction scar. *J Am Coll Cardiol*. 2015;65:2057–2066.

44. Humeres C, Frangogiannis NG. Fibroblasts in the infarcted, remodeling, and failing heart. *J Am Coll Cardiol Basic Trans Science*. 2019;4:449–467.

45. Bernardo ME, Fibbe WE. Mesenchymal stromal cells: sensors and switchers of inflammation. *Cell Stem Cell*. 2013;13:392–402.

46. Gazdic M, Volarevic V, Arsenijevic N, Stojkovic M. Mesenchymal stem cells: a friend or foe in immune-mediated diseases. *Stem Cell Rev Rep*. 2015;11:280–287.

47. Patel B, Bansal SS, Ismahil MA, et al. CCR2(+) monocyte-derived infiltrating macrophages are required for adverse cardiac remodeling during pressure overload. *J Am Coll Cardiol Basic Trans Science*. 2018;3:230–244.

48. Bonner JC. Regulation of PDGF and its receptors in fibrotic diseases. *Cytokine Growth Factor Rev*. 2004;15:255–273.

49. Heldin CH, Lennartsson J. Structural and functional properties of platelet-derived growth factor and stem cell factor receptors. *Cold Spring Harb Perspect Biol*. 2013;5:a009100.

50. Farahani RM, Xaymardan M. Platelet-derived growth factor receptor alpha as a marker of mesenchymal stem cells in development and stem cell biology. *Stem Cells Int*. 2015;2015:362753.

51. Wang X, Wu X, Zhang A, et al. Targeting the PDGF-B/PDGFR-beta interface with destruxin A5 to selectively block PDGF-BB/PDGFR-ββ signaling and attenuate liver fibrosis. *EBioMedicine*. 2016;7:146–156.

52. Lewis CC, Chu HW, Westcott JY, et al. Airway fibroblasts exhibit a synthetic phenotype in severe asthma. *J Allergy Clin Immunol*. 2005;115:534–540.

53. Neumann F, Poelitz A, Hildebrandt B, et al. The tyrosine-kinase inhibitor imatinib induces long-term remission in a patient with chronic myelogenous leukemia with translocation t(4;22). *Leukemia*. 2007;21:836–837.

54. Chong JJ, Reinecke H, Iwata M, Torok-Storb B, Stempien-Otero A, Murry CE. Progenitor cells identified by PDGFR-alpha expression in the developing and diseased human heart. *Stem Cells Dev*. 2013;22:1932–1943.

55. Yue Z, Chen J, Lian H, et al. PDGFR-beta signaling regulates cardiomyocyte proliferation and myocardial regeneration. *Cell Rep*. 2019;28:966–978.e4.

56. Kerkela R, Grazette L, Yacobi R, et al. Cardiotoxicity of the cancer therapeutic agent imatinib mesylate. *Nat Med*. 2006;12:908–916.

57. Estabragh ZR, Knight K, Watmough SJ, et al. A prospective evaluation of cardiac function in patients with chronic myeloid leukaemia treated with imatinib. *Leuk Res*. 2011;35:49–51.

58. Trent JC, Patel SS, Zhang J, et al. Rare incidence of congestive heart failure in gastrointestinal stromal tumor and other sarcoma patients receiving imatinib mesylate. *Cancer*. 2010;116:184–192.

59. van den Akker F, de Jager SC, Sluijter JP. Mesenchymal stem cell therapy for cardiac inflammation: immunomodulatory properties and the influence of toll-like receptors. *Mediators Inflamm*. 2013;2013:181020.

60. Madonna R, Van Laake LW, Davidson SM, et al. Position Paper of the European Society of Cardiology Working Group Cellular Biology of the Heart: cell-based therapies for myocardial repair and regeneration in ischemic heart disease and heart failure. *Eur Heart J*. 2016;37:1789–1798.

61. Katarzyna R. Adult stem cell therapy for cardiac repair in patients after acute myocardial infarction leading to ischemic heart failure: an overview of evidence from the recent clinical trials. *Curr Cardiol Rev*. 2017;13:223–231.

62. Iso Y, Spees JL, Serrano C, et al. Multipotent human stromal cells improve cardiac function after myocardial infarction in mice without long-term engraftment. *Biochem Biophys Res Commun*. 2007;354:700–706.

63. Pei Z, Zeng J, Song Y, et al. In vivo imaging to monitor differentiation and therapeutic effects of transplanted mesenchymal stem cells in myocardial infarction. *Sci Rep*. 2017;7:6296.

64. Amsalem Y, Mardor Y, Feinberg MS, et al. Iron-oxide labeling and outcome of transplanted mesenchymal stem cells in the infarcted myocardium. *Circulation*. 2007;116:I38–I45.

KEY WORDS cardiac remodeling, fibrosis, heart failure, mesenchymal stem cells, myocardial inflammation, myofibroblasts, platelet-derived growth factor receptor

APPENDIX For supplemental figures, please see the online version of this paper.